

SYNTHETIC AND PHOTOCHEMICAL STUDY OF RUTHENIUM  
POLYPYRIDINE SOLAR DYES COUPLED TO CADMIUM SELENIDE  
QUANTUM DOTS

---

A Thesis  
Presented to  
The Honors Tutorial College  
Ohio University

---

In Partial Fulfillment  
of the Requirements for Graduation  
from the Honors Tutorial College  
with the degree of  
Bachelor of Science in Chemistry

---

By  
Jill A. Carlson  
June 2012

This thesis has been approved by  
The Honors Tutorial College and the Department of Chemistry and Biochemistry

---

Dr. Jeffrey J. Rack  
Professor, Chemistry  
Thesis Advisor

---

Dr. Lauren E. H. McMills  
Chemistry Director of Studies  
Honors Tutorial College

---

Dr. Jeremy Webster  
Dean, Honors Tutorial College

Acknowledgements:

Many people have supported and mentored me throughout my undergraduate life. It is due to many of these people that my passion for sustainable energy systems emerged and grown. First, I want to thank my research advisor Dr. Jeffrey Rack for taking that hour of inorganic chemistry class to discuss the energy problem, for the renewable energy tutorial in fall 2009, continuing to mentor me throughout undergraduate research, and supporting me in many application processes for research funding, awards, and graduate school. Furthermore, I would like to thank Dr. Greg Van Patten and PhD student Chris McCleese for helpful discussions and instruction with the nanocrystal quantum dot portion of my project as well as providing so graciously several different sizes of nanocrystal quantum dots for my use. I would like to thank the Provost's Undergraduate Research Fund for research funding.

Furthermore, Dr. Nancy Manring, Dr. Steve Scanlan, Sonia Marcus, and Annie Laurie Cadmus all contributed to the "environmental" complement to my studies and, therefore, I owe them much breadth of knowledge and growth in critical thinking in institutional sustainability and energy policy. I want to thank my lab group for challenging me in my abilities as well as making the lab as fun, humorous, and unpredictable as possible. I want to thank Dr. Lauren McMills and the Honors Tutorial College for their continued encouragement and wisdom. Finally, I want to thank my mom, Lorena Carlson, for supporting me throughout all of these 5 years while I waxed and waned between being tired and manically ready to do everything and anything I could get my hands on.

*The noblest of all studies  
is the study of what man is and  
of what life he should live.*

Plato

*For my dad: the late Dr. William Carlson, D.O.*

*For instilling in me at an early age, a fascination of science and love of public service*

**TABLE OF CONTENTS:**

<b>INTRODUCTION</b> .....	10
Current Global Energy Use.....	10
Impacts from Fossil Fuels.....	12
Seeking Alternatives: Solar Energy .....	14
Dye Sensitized Solar Cells.....	17
Two-Fold Research Aim .....	18
<b>EXPERIMENTAL</b> .....	21
Instrumentation.....	21
Materials.....	22
Syntheses.....	23
Tris-Heteroleptic Ruthenium Solar Dyes.....	23
Synthesis of [Ru(p-cymene)Cl <sub>2</sub> ] <sub>2</sub> .....	23
Synthesis of [Ru(p-cymene)bpyCl]Cl .....	24
Synthesis of [Rubpy(bpy(COOH) <sub>2</sub> )Cl <sub>2</sub> ] .....	25
Synthesis of [Rubpybpy'OS] .....	26
Synthesis of [Rubpy(bpy(CO <sub>2</sub> CH <sub>2</sub> CH <sub>3</sub> ) <sub>2</sub> )Cl <sub>2</sub> ] .....	27
Synthesis of Rubpy(bpy(CO <sub>2</sub> CH <sub>2</sub> CH <sub>3</sub> ) <sub>2</sub> )OS] .....	28
Synthesis of [Ru(p-cymene)dmbCl]Cl.....	29
Synthesis of [Rudmb(bpy(CO <sub>2</sub> CH <sub>2</sub> CH <sub>3</sub> ) <sub>2</sub> )Cl <sub>2</sub> ].....	30
Synthesis of [Rudmb(bpy(CO <sub>2</sub> CH <sub>2</sub> CH <sub>3</sub> ) <sub>2</sub> )Cl <sub>2</sub> ].....	31
Synthesis of [Ru(p-cymene)biqCl]Cl .....	32

Synthesis of [Rubiq(bpy(CO <sub>2</sub> CH <sub>2</sub> CH <sub>3</sub> ) <sub>2</sub> )Cl <sub>2</sub> ]	33
Synthesis of [Rubiq(bpy(CO <sub>2</sub> CH <sub>2</sub> CH <sub>3</sub> ) <sub>2</sub> )OS]	34
Ruthenium Adducts for CdSe Quantum Dot Assemblies	35
Synthesis of 4,4'-di(3-chloropropyl)-2,2'-bipyridine	35
Synthesis of 2,2'-bipyridine-4,4'-dithioacetate	37
Synthesis of [Ru(bpy) <sub>2</sub> (bpySAc)](PF <sub>6</sub> ) <sub>2</sub>	38
Synthesis of	
[Ru(bpy) <sub>2</sub> (4,4'-dithiopropyl-2,2'-bipyridine)](PF <sub>6</sub> ) <sub>2</sub>	39
Photochemical Studies Sample Preparation: Steady State	
Luminescence	40
Coupled with CdSe NQDs (2.5 nm diameter)	40
<b>RESULTS AND DISCUSSION</b>	42
Part I: Tris-Heteroleptic Solar Dyes: Synthetic Problems and Solutions	42
Brief Absorbance Spectra Analysis	49
Part II: Photochemical Analysis of Ruthenium and Quantum Dot	
Assemblies	52
Experiment 1: Coupling with 2.5 nm CdSe NQDs	
in lower concentrations	55
<b>CONCLUSIONS AND FUTURE DIRECTIONS</b>	62
<b>REFERENCES</b>	64

**Table of Figures:**

Figure 1: Schematic of Dye Sensitized Solar Cell Architecture

Figure 2: Molecular structure of  $[\text{Ru}(\text{bpy})_2(4,4'\text{-dithiopropyl-2,2'}\text{-bipyridine})](\text{PF}_6)_2$

Figure 3: Synthetic scheme for  $[\text{Ru}(\text{p-cymene})\text{Cl}_2]_2$

Figure 4: Synthetic scheme for  $[\text{Ru}(\text{p-cymene})\text{bpyCl}]\text{Cl}$

Figure 5: Synthetic scheme for  $[\text{Ru}(\text{bpy}(\text{COOH})_2)\text{Cl}_2]$

Figure 6: Synthetic scheme for  $[\text{Ru}(\text{bpy}(\text{CO}_2\text{CH}_2\text{CH}_3)_2)\text{OS}](\text{PF}_6)$  (PF<sub>6</sub> counterions omitted)

Figure 7: Synthetic scheme for  $[\text{Ru}(\text{bpy}(\text{CO}_2\text{CH}_2\text{CH}_3)_2)\text{Cl}_2]$

Figure 8: Synthetic scheme for  $[\text{Ru}(\text{bpy}(\text{CO}_2\text{CH}_2\text{CH}_3)_2)\text{OS}](\text{PF}_6)_2$

Figure 9: Synthetic scheme for  $[\text{Ru}(\text{p-cymene})\text{dmbCl}]\text{Cl}$

Figure 10: Synthetic scheme for  $[\text{Ru}(\text{dmb}(\text{bpy}(\text{CO}_2\text{CH}_2\text{CH}_3)_2)\text{Cl}_2)]$  (DMF)

Figure 11: Synthetic scheme for  $[\text{Ru}(\text{dmb}(\text{bpy}(\text{CO}_2\text{CH}_2\text{CH}_3)_2)\text{Cl}_2)]$  (propylene carbonate)

Figure 12: Synthetic scheme for  $[\text{Ru}(\text{p-cymene})\text{biqCl}]\text{Cl}$

Figure 13: Synthetic scheme for  $[\text{Ru}(\text{biq}(\text{bpy}(\text{CO}_2\text{CH}_2\text{CH}_3)_2)\text{Cl}_2]$

Figure 14: Synthetic scheme of  $[\text{Ru}(\text{biq}(\text{bpy}(\text{CO}_2\text{CH}_2\text{CH}_3)_2)\text{OS}](\text{PF}_6)_2$

Figure 15: Synthetic scheme for 4,4'-di(3-chloropropyl)-2,2'-bipyridine

Figure 16: Synthetic scheme for 2,2'-bipyridine-4,4'-dithioacetate (bpySAc)

Figure 17: Synthetic scheme for  $[\text{Ru}(\text{bpy})_2(\text{bpySAc})](\text{PF}_6)_2$

Figure 18: Synthetic scheme for

$[\text{Ru}(\text{bpy})_2(4,4'\text{-dithiopropyl-2,2'}\text{-bipyridine})](\text{PF}_6)_2$

Figure 19: Two of the original target solar dye complexes

Figure 20: Molecular structure of pyS ligand and problematic solar dye complex

Figure 21: General synthetic scheme for  $[\text{Ru}(\text{p-cymene})\text{Cl}_2]_2$  dimer to  $[\text{Ru}(\text{bpy})(\text{p-cymene})\text{Cl}]\text{Cl}$  synthesis

Figure 22: General synthetic scheme for  $[\text{Ru}(\text{bpy})(\text{p-cymene})\text{Cl}]\text{Cl}$  complex to  $[\text{Ru}(\text{bpy})(\text{bpy}')\text{Cl}_2]$

Figure 23:  $^1\text{H-NMR}$  aromatic region of 4,4'-dimethyl-2,2'-bipyridine

Figure 24:  $^1\text{H-NMR}$  aromatic region of 2,2'-bipyridine

Figure 25:  $^1\text{H-NMR}$  aromatic region of 2,2'-biquinoline

Figure 26: Comparison of absorbance spectra of  $[\text{Ru}(\text{bpy})_3]^{2+}$  and  $[\text{Ru}(\text{bpy})(\text{bpy}')\text{OS}](\text{PF}_6)$

Figure 27: Absorbance spectra showing progression from  $[\text{Ru}(\text{p-cymene})\text{Cl}_2]_2$  dimer starting complex to  $[\text{Ru}(\text{bpy})(\text{bpy}')\text{OS}]$

Figure 28: Absorbance spectra of  $[\text{Ru}(\text{bpy})_2(4,4'\text{-dithiopropyl-2,2'\text{-bipyridine})](\text{PF}_6)_2$ , Cadmium Selenide Nanocrystal Quantum Dots, and the mixture

Figure 29: Steady State Photoluminescence of  $[\text{Ru}(\text{bpy})_2(4,4'\text{-dithiopropyl-2,2'\text{-bipyridine})](\text{PF}_6)_2$ , excitation at 400 nm

Figure 30: Steady State Photoluminescence of  $[\text{Ru}(\text{bpy})_2(4,4'\text{-dithiopropyl-2,2'\text{-bipyridine})](\text{PF}_6)_2$ , excitation 500 nm

Figure 31: Schematic of electron excitation via light absorption and subsequent hypothesized hole transfer to the ruthenium complex

Figure 32: Steady State Photoluminescence of  $[\text{Ru}(\text{bpy})_2(4,4'\text{-dithiopropyl-2,2'}\text{-bipyridine})](\text{PF}_6)_2$  and Cadmium Selenide NQD mixture compared to CdSe NQD emission, excitation at 400 nm

Figure 33: Steady State Photoluminescence of  $[\text{Ru}(\text{bpy})_2(4,4'\text{-dithiopropyl-2,2'}\text{-bipyridine})](\text{PF}_6)_2$  and Cadmium Selenide NQD mixture compared to CdSe NQD emission, excitation at 500 nm

## INTRODUCTION

### Current Global Energy Use

The single biggest challenge of our century is efficiently and cost-effectively powering our lives while protecting the environment and mitigating global climate change.<sup>1,2,3,4</sup> Arguably, no quandary has ever had the potential to impact more people over a longer period of time than our current energy crisis may have, if sustainable solutions are not implemented on the local and global scale, for the urban, suburban, and rural dweller, and for the developed and developing world.

We currently are at a crossroads. In the last 50 years, the world's population has more than doubled from 3 billion people in 1960 to 7 billion people in 2012.<sup>5</sup> While populations continue to grow, more and more people are gaining access to life-enhancing technologies. However, despite the industrial and technological revolutions of the last three centuries, many are lacking basic human needs such as adequate shelter, clean water and food, or an education. The conundrum lies in how to continue to improve quality of life for the short term while ensuring a healthy, prosperous future for later generations. Furthermore, while the developing world transforms into energy intensive consumers, many developed nations are facing an aging infrastructure.<sup>4</sup> Finally, it is estimated that the worldwide demand for energy will double by 2050 and triple by the end of the century,<sup>6</sup> with population expected to grow to at least 9 billion humans by 2050.<sup>5</sup>

The developed first world's activities and populations are supported by an extensive energy distribution network that is powered by nonrenewable fossil fuels. Truly every aspect of life is supported by energy in one form or another. Domestically, the United States utilizes petroleum, which accounts for approximately 37% of total energy use, predominantly for transportation. Natural gas accounts for the second largest contributor to our energy stream, 24% of total energy use, and is funneled rather equally into residential and commercial purposes, the industrial sector, and electricity power generation. Coal accounts for approximately 21% of our total fossil fuel use, but almost all – 94% – is utilized for electricity generation. The remaining energy sources consist of nuclear power and renewable energies with 9% and 8% respectively. Although the disadvantages to these fuel sources exist even when minimally implemented, these proportions become extremely problematic *due* to the extent and breadth of scale. If every human on the planet Earth lived by the standards of an average American, we would need approximately three planet earths' worth of resources to sustain life.<sup>8</sup>

Globally, the distribution of energy sources is similar with roughly 85% representing the fossil fuels of oil, gas, and coal in approximately equal parts. Unsustainable biomass and nuclear power are the largest other portions of the energy pie. Finally, hydroelectric energy generation is consumed on the same scale that all other combined renewable energies are implemented at approximately 8%.<sup>2,3,7</sup> Despite the high proportion of energy that comes from carbon free nuclear and hydroelectric power, there are several factors that are limiting the growth of these two energies.

Hydroelectric power capacity and generation has remained constant for the past decade.<sup>9</sup> Although nuclear energy is a carbon-free alternative with an immense energy output, many argue that this fossil fuel alternative still has serious waste remediation and diversion issues. Furthermore, other recent global events have provoked citizens, institutions, and governments to rethink humanity's ability to prevent and mitigate nuclear plant disasters. Most significantly, the Fukushima Nuclear Power Plant disaster in Japan and the 25<sup>th</sup> anniversary of the Chernobyl Nuclear Power Plant Meltdown in 2011 are saddening reminders of humanity's inability to safeguard against all plant failures. The role of nuclear power globally is in huge flux. While the United States proceeds with plans to build new small reactors, Germany and Switzerland – both industrialized nations – have decided to terminate their nuclear programs and transition to a more renewable energy portfolio.

### **Impacts from Fossil Fuels**

The environmental impacts of fossil fuels are detrimental throughout the entirety of their lifecycles. Ever more invasive extraction methodologies are further externalizing the costs of these finite power sources. Additionally, human and environmental health is compromised due to air and water pollution caused by oil, coal, and natural gas combustion. Namely, the oil and natural gas industry is the largest industrial source of volatile organic compounds (VOCs) and emits the greenhouse gas methane as well as carcinogens benzene and hexanes. VOCs combine

with nitrous oxides in the air to form ground level or tropospheric ozone which when inhaled compromises human health.<sup>10</sup>

Additionally burning coal creates emissions of carbon dioxide, sulfur dioxide, nitrous oxides, and mercury compounds. Mercury containing compounds are an environmental and human health hazard. Mercury compounds can bioaccumulate in the environment and even at minimal concentrations can be toxic.<sup>11</sup> The atmospheric concentrations of greenhouse gases including carbon dioxide, methane, and nitrous oxide have not only steadily risen from pre-industrial values,<sup>12</sup> but also have been the highest ever in the last 650,000 years. Most notably, carbon dioxide atmospheric concentrations have risen from approximately 280 to unprecedented numbers of 395 parts per million (ppm) reported in April 2012.<sup>13,14</sup> These rising carbon dioxide, methane, and nitrous oxide emissions have direct roles in climate change.

Global climate change risks further environmental disruption with significant changes in precipitation and temperature.<sup>15</sup> These changes in precipitation and temperature as well as more extreme weather conditions will alter land use. Biogeographically, plant and animal ranges will change or completely disappear.<sup>15</sup> These changes in geographic distributions will only further strain species. Currently, the planet earth is experiencing species extinction events at a rate 1,000 or more times higher than historic records.<sup>16,17</sup>

Although the atmospheric concentration of carbon dioxide is most often the focus of climate change discussion, the ocean also serves as a carbon dioxide sink, having absorbed approximately one-half of the carbon dioxide produced by industrial

processes. This carbon dioxide absorption has altered the ocean's natural carbonate system due to acidification,<sup>15</sup> leading to declines in corals and other marine calcifiers. Further strain on natural resources will further political conflict and societal strife. Natural resources, both those essential to life and those that serve roles in power and commerce, fuel war both directly and indirectly.<sup>18</sup> Simply, scarcity of natural resources is destabilizing to society. Conflict over resources then furthers ecological destruction, only exacerbating the natural resource scarcity.<sup>18</sup> Economies that are based primarily in a natural resource industry are highly volatile due to supply and demand changes. These fluctuations weaken the respective society and government. Poor quality of life increases the risk of conflict and conflict weakens human development in a positive feedback loop.<sup>18</sup>

Despite the overwhelming nature of these problems, there is much hope in our collaborative capabilities as people and institutions to work toward solutions. History provides several examples of triumphs over what appear to be insurmountable environmental and societal struggles. Our ability to transition to energy alternatives is limited only by the idea that we should proceed in our current trajectory, not questioning how we should live.

### **Seeking Alternatives: Solar Energy**

Reflecting upon these pressing environmental, social, and economic factors, a reduction of fossil fuel use must be accomplished. Although the cultural paradigm should embrace conservation and efficiency, the implementation of alternative

energies will have the largest impact on our environmental footprint and rightly must be demanded. One such option that is being rigorously explored is solar power. More energy from the sun falls on the earth in one hour than is used by the 7 billion strong world's population in one year.<sup>4</sup> Despite the reality that capturing this energy source efficiently and cost-effectively is an extremely difficult research and development question, the sheer immensity of energy contained in the radiation of a star approximately 93,000,000 miles away is remarkable.<sup>20</sup>

Solar power is defined as the energy that is directly captured from the sun's radiation.<sup>21</sup> Capturing the energy can be accomplished in two basic fashions: solar thermal devices use concentrated sunlight to directly heat water or to generate steam to drive turbines. Also, solar energy can be directly converted to electricity using a photovoltaic (PV) device.<sup>22</sup>

During PV and solar thermal manufacture, caustic reagents are utilized and wastes produced; however, during its *full* lifetime, solar energy is greenhouse gas emission and air pollutant free.<sup>21</sup> Solar energy, although fluctuating throughout the day, predominantly parallels people's energy consumption load peaks. Solar energy is a "democratic" energy source. Although solar energy fluctuates on a temporal and spatial scale, it is not a source whose "potential" knows state, national, or continental boundaries. Observing a map of world oil production, the political and economic ramifications of the petroleum trade become clear. Although the United States biggest importers of crude oil are the physical neighbors Canada and Mexico, politically and economically, the country is entangled with many nations with the highest known oil

reserves: namely Saudi Arabia, Iran, and Iraq.<sup>23</sup> The ubiquity of solar energy promotes economic independence and political stability. Solar energy is a clean, abundant, renewable energy source.

Despite the multitude of reasons to transition from finite fossil fuels to solar-based alternatives (amongst a diverse variety of sustainable energy sources), current technologies to harness sunlight are at a high cost and therefore not competitive on a commercial scale. The cost of solar energy generated electricity has exponentially decreased over the past 30 years,<sup>24</sup> yet more work is yet to be done. On *several* frontiers, photovoltaic device materials and architectures are being created and designed.<sup>25</sup> Generally, photovoltaic devices incorporate a type of semiconductor for generation of electrical current through photo irradiation. The solar radiation spreads from the ultraviolet (UV) to infrared (IR) regions of the electromagnetic spectrum or 300 – 900 nm wavelength light. This wavelength range corresponds to band gaps of 0.5 – 3.5 eV.<sup>6</sup>

Several different photovoltaic schemes exist from crystalline silicon to thin film devices that incorporate amorphous silicon, cadmium telluride, or copper indium gallium selenium (CIGS) heterojunctions.<sup>25</sup> When extraction costs and supply constraints are considered, a multitude of other light absorbing materials start to become economically feasible if they can be cheaply processed.<sup>25</sup> Namely, the exploration of novel chromophores or dye sensitizers, different processing and deposition techniques,<sup>25</sup> new redox couples, nanomaterials and polymers,<sup>26</sup> and various architectures from single junction to heterojunction systems is taking place.<sup>27</sup>

## Dye Sensitized Solar Cells

One architecture that has been extensively studied is the dye sensitized solar cell (DSSC). The DSSC architecture drastically differs from the bulk silicon photovoltaic scheme in which both light absorption and charge separation occur in the semiconductor. This DSSC scheme was introduced by Gratzel and O'Regan in a seminal paper published in *Nature* in 1991. In this work, a high surface area, mesoporous titanium dioxide ( $\text{TiO}_2$ ) thin film is sensitized by a ruthenium polypyridyl dye that acts to harvest light and efficiently charge inject into the conduction band of the  $\text{TiO}_2$  layer. Finally, the oxidized dye is regenerated by electron transfer from a redox species in solution: an  $\text{I}_3^-/\text{I}^-$  couple. The ruthenium sensitizers in the shaping work included the named N3 and N719 dyes, which involve carboxylate-derivatized polypyridyl and thiocyanate ligands. These “black” dyes are highly absorbent in the visible region and strongly couple to the  $\text{TiO}_2$  substrate through their carboxylate moieties. Furthermore, the ruthenium dyes have enough of a thermodynamic drive to charge inject into the conduction band of the titania.

A schematic of the DSSC is shown in Figure 1. The figure shows the desired processes of 1) electron excitation via photon absorption, 2) charge injection, 3) charge collection, and 4) electron transfer to regenerate ground state ruthenium dye. This schematic does not demonstrate the other processes that can occur including radiative and nonradiative decay and electron leaking. This work proved critical due to its novelty in construction, use of low to medium-purity materials, and its high conversion efficiencies. The overall light-to electric energy conversion yield was 7.1 –

7.9% in simulated solar light<sup>28</sup> and since 1991 has simply plateaued at reported efficiencies of 11%.<sup>7</sup>

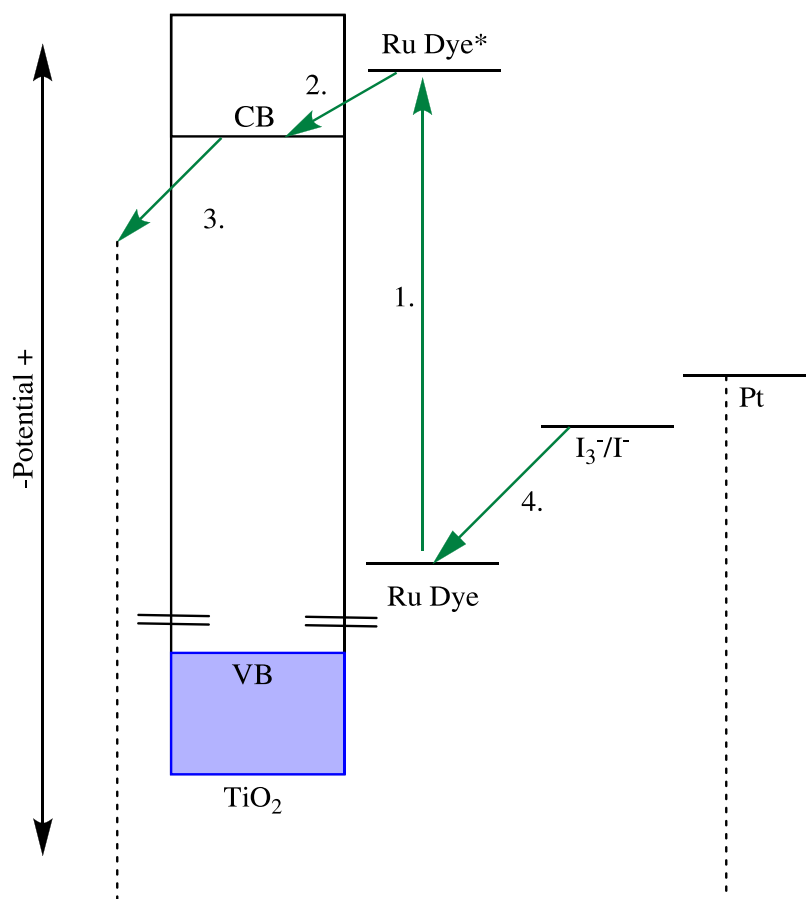


Figure 1: Schematic of Dye Sensitized Solar Cell Architecture

### Two-Fold Research Aim

The goal of this research product was to synthesize and characterize novel ruthenium complex molecular systems for solar energy capturing purposes. The research product took two distinct, yet related paths. First, syntheses of tris-heteroleptic (containing 3 different ligands) ruthenium polypyridyl complexes were explored for use in dye-sensitized solar cell architectures. Second, the interfacial

electron transfer of a ruthenium complex-cadmium selenide quantum dot assembly was studied using UV-Vis absorbance and fluorescence spectroscopy.

Ruthenium polypyridine dyes serve as good photosensitizers in dye sensitized solar cells as they absorb strongly in the visible region, are stable upon irradiation, and have the fitting HOMO (Highest Occupied Molecular Orbital)-LUMO (Lowest Unoccupied Molecular Orbital) gap potential for easy quenching of excited states. Also, they have a relatively wide window of redox inertness of the ruthenium metal. Furthermore, the LUMO is ligand dependent and therefore can be tuned by alteration of ligands. These syntheses were optimized to be facile and efficient in creating highly pure samples of ruthenium complexes to be used as highly absorbant sensitizers.<sup>29,30,31</sup>

Secondly, a novel ruthenium polypyridyl complex was synthesized and coupled with cadmium selenide nanocrystal quantum dots (CdSe NQDs). Several studies have been undertaken that explore the interfacial electron dynamics of coupled small molecule – nanocrystal quantum dot assemblies.<sup>32,33,34,35,36,37</sup> At the core of all of these research endeavours is exploring the rate of adsorption of the small molecule-NQD assembly and the energy transfer mechanism. The rate of excited state relaxation and electron/hole delocalization are explored through several different tools including <sup>1</sup>H-NMR, absorbance, steady state and time-resolved photoluminescence, nanosecond transient absorption, and femtosecond transient absorption spectroscopy. Although these molecular components have implications for the solid state photovoltaic devices, this project, similar to many others, involves solution-based studies.<sup>32, 33, 34, 35, 36,37</sup>

Certainly, the breadth of research within the realm of this interface demonstrates the nontrivial partner of the nanocrystal quantum dot. Nanocrystal quantum dots are crystalline lattices of semiconductor materials that exhibit size-dependent optical and electronic properties. The size-dependent properties emerge from the “0” dimension box that the quantum dot could be visualized as. Simply, the excitons – or electron-hole pairs – contained in the semiconductor are confined at the nano-scale. They exhibit a high surface area to volume ratio. They are broad absorbers in the ultraviolet and visible spectrum, with high extinction coefficients, and feature intense emission. The nanocrystal quantum dots contain cores of semiconductor metals (in this study, cadmium and selenium forming a II-IV junction) stabilized by long amphiphilic capping agents. These capping agents, such as trioctylphosphine oxide (TOPO) and hexadecylamine prevent quantum dot aggregation and further growth as well as allow solvation of the crystals in various solvents. The sizes of cadmium selenide (CdSe) quantum dots range from 2 – 10 nm in diameter and have corresponding maximum wavelength of absorbance values within the visible spectrum.<sup>38,39,40</sup>

The ruthenium polypyridyl complex exhibits terminal sulfur linkages as shown below in Figure 2. Many of the molecules adsorbed to the nano-scale semiconductors utilize carboxylate or amine functional groups that couple to the surface via electrostatic affinity or physical crystalline matrix incorporation. Therefore, terminal sulfur groups are hypothesized to more readily couple with the cadmium selenide

nanocrystal quantum dot, due to the softness of the sulfur and more similar valence to the selenium.

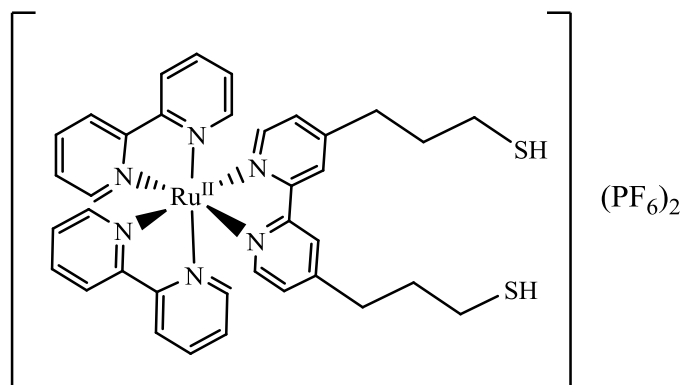


Figure 2: Molecular Structure of  $[\text{Ru}(\text{bpy})_2(4,4'\text{-dithiopropyl-}2,2'\text{-bipyridine})](\text{PF}_6)_2$

The photochemistry of this coupled ruthenium (Ru) metal complex – CdSe NQD assembly was studied for its application in a solar energy device due to the potential for an ultrafast charge separator junction forming between the two species.

## EXPERIMENTAL

### Instrumentation

One dimensional  $^1\text{H-NMR}$  and  $^{13}\text{C-NMR}$  were collected on a 300 MHz Bruker AG spectrometer. Electronic absorption spectra were collected on an Agilent 8453 spectrophotometer. Steady-state luminescence was collected on a PTI-C60 fluorimeter equipped with a Hamamatsu R928 PMT (185-900 nm).

## Materials

The reagent  $\text{Ru(III)Cl}_3 \cdot \text{H}_2\text{O}$  was purchased from Strem Chemicals. The reagent 2,2'-biquinoline was purchased from Alfa Aesar. The reagents 4,4'-diethylester-2,2'-bipyridine and 4,4'-dicarboxylic acid-2,2'-bipyridine were synthesized and isolated by fellow PhD graduate student Yuhuan Jin. The reagent  $[\text{Ru}(\text{bpy})_2\text{Cl}_2] \cdot 2\text{H}_2\text{O}$  was synthesized and isolated by fellow PhD graduate student Albert King. All other reagents were purchased from Sigma-Aldrich Co. All reagents were utilized as received unless otherwise noted.

The solvents acetone, acetonitrile, chloroform, dichloromethane, ethanol, ethyl acetate, hexanes, and methanol and the reagent anhydrous  $\text{MgSO}_4$  were purchased from VWR International and used without further purification unless otherwise noted. The reagents ammonium hydroxide and anhydrous ethyl ether were obtained from Fisher Scientific. All deuterated NMR solvents were purchased from Cambridge Isotope Laboratories, Inc. The solvent *N,N'*-dimethylformamide was obtained from Sigma-Aldrich Co.

The dry tetrahydrofuran was obtained from Dr. Stephen Bergmeier's organic chemistry laboratory group. The diphenylacetic acid was obtained from Dr. Mark McMills' organic chemistry laboratory group. Cadmium selenide quantum dots were obtained from Dr. Greg Van Patten's laboratory group and exchanged rightfully for ruthenium polypyridyl complexes from our laboratory.

## Tris-Heteroleptic Ruthenium Solar Dyes

### Synthesis of $[\text{Ru}(\text{p-cymene})\text{Cl}_2]_2$

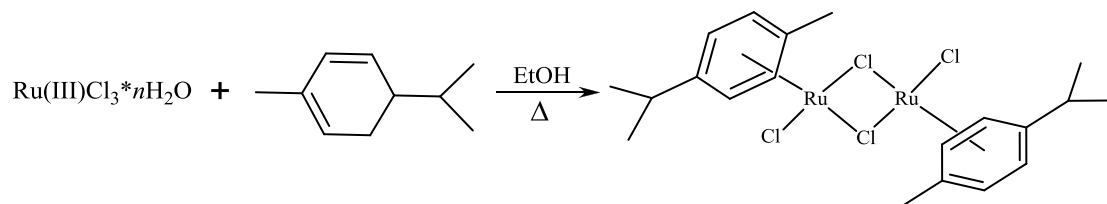


Figure 3: Synthetic scheme for  $[\text{Ru}(\text{p-cymene})\text{Cl}_2]_2$

In a 24/40 neck 250 mL round bottom flask, equipped with a stir bar, 100 mL of ethanol were purged with nitrogen gas. To the solution, 8 mL ( $\rho$ : 0.846 g/cm<sup>3</sup>, FW: 136.23 g/mol, 0.050 mol) of  $\alpha$ -phellandrene were added. Then 1.57 g (FW: 207.43 (anhydrous) g/mol, 40-43% Ru, 0.0076 mol) of  $[\text{Ru}^{\text{III}}\text{Cl}_3] \cdot x\text{H}_2\text{O}$ , were dissolved in the flask. The reaction mixture was refluxed under nitrogen for 4 hours. Afterward, the solution was reduced to  $\frac{1}{4}$  of the volume via rotary evaporation. To assist in the product precipitation, 15 mL of anhydrous ethyl ether were added and placed in the freezer overnight. The precipitated product was isolated via vacuum filtration on a 30 mL medium frit to afford a brown-red crystalline solid. Yield: 1.63 g (77%). UV-vis ( $\text{CH}_3\text{OH}$ )  $\lambda_{\text{max}} = 433$  nm. <sup>1</sup>H NMR ( $\text{CD}_3\text{CN}$ , 300MHz)  $\delta$ : 5.564 (d, 1H), 5.315 (d, 2H), 2.951 (m, 2H), 2.221 (s, 3H), 1.305 (d, 6H) ppm.

### Synthesis of [Ru(p-cymene)bpyCl]Cl

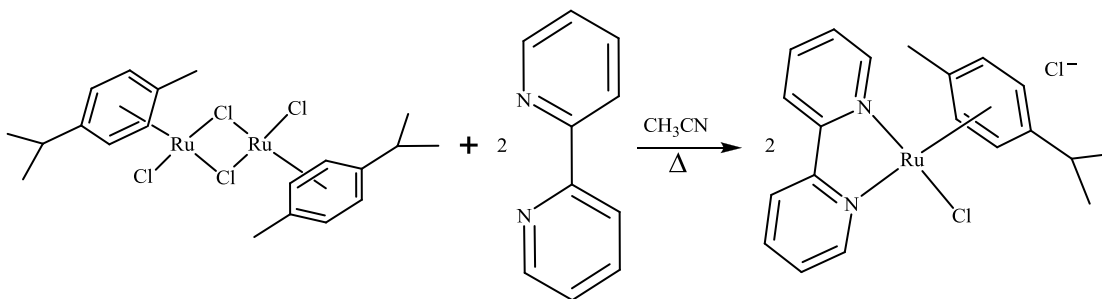


Figure 4: Synthetic scheme for [Ru(p-cymene)bpyCl]Cl

In a 14/20 neck 10 mL round bottom flask, equipped with a stir bar, 4 mL acetonitrile (CH<sub>3</sub>CN) were purged with nitrogen. To the sparged solution, 374 mg (FW: 612.39, 0.611 mmol) of the [Ru(p-cymene)Cl<sub>2</sub>]<sub>2</sub> dimer were dissolved along with 214 mg (FW: 156.18 g/mol, 1.37 mmol) of 2,2'-bipyridyl (bpy). The reaction mixture was refluxed under nitrogen for 2 hours. Shortly after combining, a bright yellow precipitate fell out of solution and continued to form throughout refluxing. After cooling to room temperature, the dark brown supernatant solution was pipetted from the round bottom. Then the bright yellow precipitate and remaining solvent were filtered on a 30 mL medium frit via vacuum filtration. The product was furthermore washed with 5 mL of CH<sub>3</sub>CN and left to dry on the frit. Yield: 523 mg (92.4%). UV-vis (CH<sub>3</sub>CN)  $\lambda_{\text{max}}$  = 346 nm. <sup>1</sup>H NMR (CD<sub>3</sub>CN, 300MHz)  $\delta$ : 9.361 (d, 2H), 8.374 (d, 2H), 8.195 (t, 2H), 7.707 (t, 2H), 5.952 (d, 2H), 5.774 (d, 2H), 2.686 (m, 1H), 2.228 (s, 3H), 1.056 (d, 6H) ppm.

### Synthesis of [Rubpy(bpy(COOH)<sub>2</sub>)Cl<sub>2</sub>]

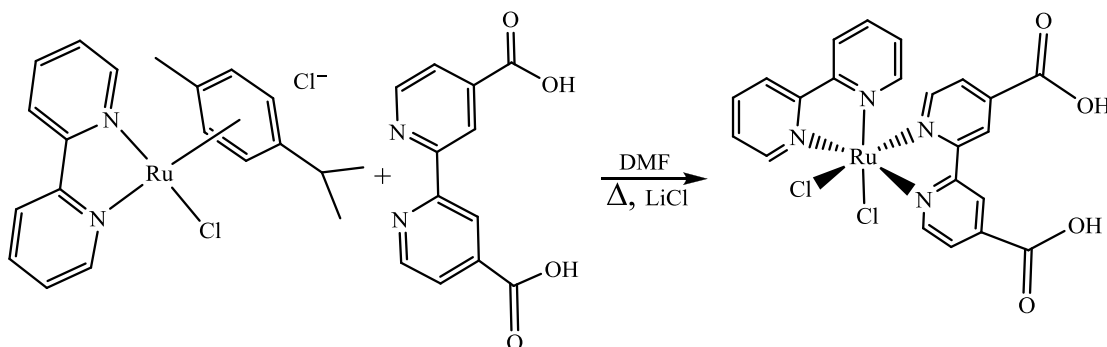


Figure 5: Synthetic scheme for [Rubpy(bpy(COOH)<sub>2</sub>)Cl<sub>2</sub>]

In a 14/20 neck 25 mL conical flask, equipped with a long, skinny stir bar, 2.5 mL of DMF were purged with nitrogen. To the purged solution, 210 mg (FW: 462.32 g/mol, 0.45 mmol) [Ru(p-cymene)bpyCl]Cl were added along with 125 mg (FW: 244.20 g/mol, 0.51 mmol) of 2,2'-bipyridine-4,4'-dicarboxylic acid (bpy'). Finally, an excess of 8 equivalents of lithium chloride (164 mg, FW: 42.39 g/mol, 3.88 mmol) were added. The reaction mixture was refluxed under nitrogen for 3 hours, during which the bright yellow reagent mixture changed from a green-brown color to finally black. Reaction mixture was cooled to room temperature and crashed with acetone. Rather than pipetting acetone into conical flask, the room temperature DMF reaction mixture was poured into a 250 mL Erlenmeyer flask filled with approximately 75 mL acetone. The mixture was then filtered on a 30 mL fine frit, washed with acetone, and dried on the vacuum line to afford a black powdery product. Yield: 224.7 mg (90.9%)

UV-vis (CH<sub>3</sub>OH)  $\lambda_{\text{max}} = 538 \text{ nm}$ .

### Synthesis of [Rubpybpy'OS]

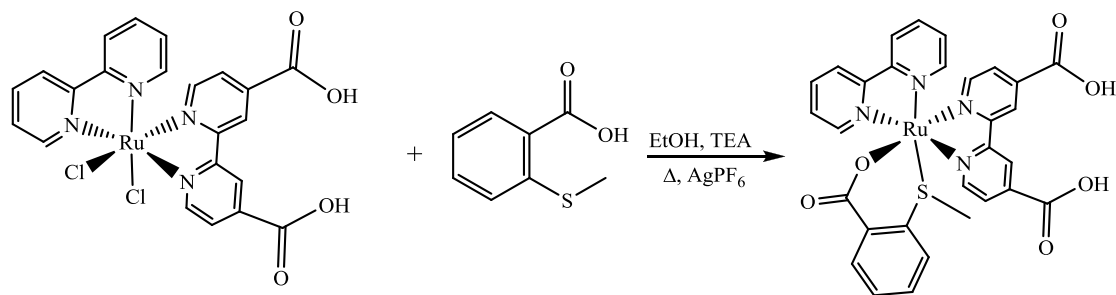


Figure 6: Synthetic scheme for [Rubpybpy'OS] (PF<sub>6</sub> counterions omitted)

In a 24/40 neck 50 mL round bottom flask, equipped with a stir bar, 25 mL of a 90/10 ethanol:H<sub>2</sub>O were purged with nitrogen. To the purged ethanol, 300 mg (FW: 572.36 g/mol, 0.52 mmol) of [Rubpybpy'Cl<sub>2</sub>], 104.7 mg (FW: 168.21 g/mol, 0.64 mmol) of 2-(Methylthio)benzoic acid, 200  $\mu$ L (FW: 101.19 g/mol,  $\rho$ : 0.726 g/mL, 1.43 mmol) of triethylamine, and 292 mg (FW: 252.83 g/mol, 1.15 mmol) of AgPF<sub>6</sub> were added. The reaction mixture was brought to reflux for 5 hours.

After cooling to room temperature, excess AgPF<sub>6</sub> was crashed with 1-2 drops of concentrated NaCl solution and placed in the freezer overnight. Grey AgCl precipitate was then filtered on a 15 mL fine frit. The red-orange ethanolic solution was then crashed with acetone and filtered on a 30 mL medium frit. The dark red-black filtrand was sticky and recrystallized with hot ethanol. The filtrate was concentrated via rotary evaporation and filtered again with acetone to afford more [Rubpybpy'OS] product. Product that was unable to be scraped due to texture was left to dry completely on frits. After 7 days, remaining product was successfully scraped to afford a highly crystalline black product. UV-vis (CH<sub>3</sub>OH)  $\lambda_{\text{max}}$  = 459 nm.

### Synthesis of [Rubpy(bpy(CO<sub>2</sub>CH<sub>2</sub>CH<sub>3</sub>)<sub>2</sub>)Cl<sub>2</sub>]

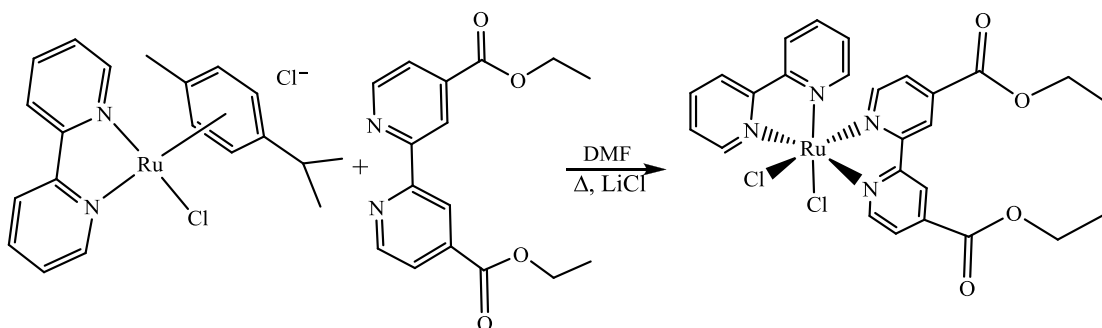


Figure 7: Synthetic scheme for [Rubpy(bpy(CO<sub>2</sub>CH<sub>2</sub>CH<sub>3</sub>)<sub>2</sub>)Cl<sub>2</sub>]

In a 14/20 neck 25 mL conical flask, equipped with a long, slender stir bar, 2.5 mL of DMF were purged with nitrogen gas. To the purged solution, 200 mg (FW: 462.32 g/mol, 0.43 mmol) [Ru(p-cymene)(bpy)Cl]Cl were added along with 156 mg of 2,2'-bipyridyl-4,4'-diethyl ester. Finally, in excess of 8 equivalents of LiCl (FW: 42.39 g/mol, 170 mg) were added to drive the reaction. Reaction mixture was refluxed under nitrogen gas for 3 hours, during which the bright yellow reagent mixture changed to black. Reaction mixture was cooled to room temperature and crashed with acetone.

Rather than pipetting acetone into conical flask, the room temperature DMF reaction mixture was directly poured into a 250 mL Erlenmeyer flask filled with approximately 75 mL of cold acetone. Mixture was then filtered on a 30 mL fine frit, washed with acetone, and dried on the frit overnight to afford a powdery product. The product was recrystallized with hot 1-butanol and filtered on a 30 mL medium frit to afford a dark black powdery solid. Yield: 284.7 mg (more than calculated yield: 283.8 mg, due to absorbed DMF). UV-vis (CH<sub>3</sub>OH)  $\lambda_{\text{max}}$  = 540 nm.

### Synthesis of Rubpy(bpy(CO<sub>2</sub>CH<sub>2</sub>CH<sub>3</sub>)<sub>2</sub>)OS]

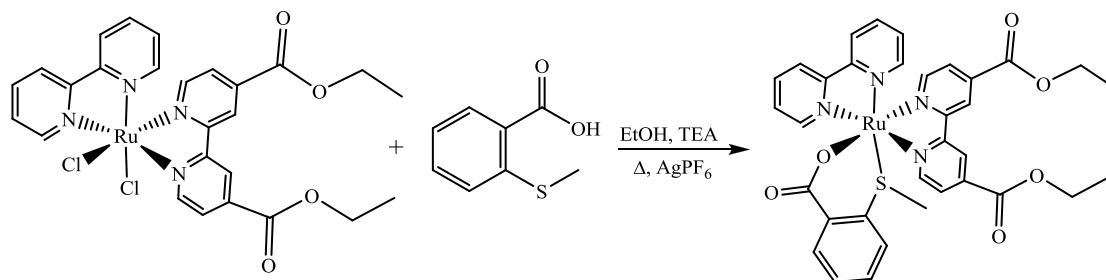


Figure 8: Synthetic scheme for [Rubpy(bpy(CO<sub>2</sub>CH<sub>2</sub>CH<sub>3</sub>)<sub>2</sub>)OS](PF<sub>6</sub>)<sub>2</sub> (PF<sub>6</sub> counterions omitted)

In a 14/20 neck 25 mL round bottom flask, 20  $\mu$ L (FW: 101.19 g/mol,  $\rho$ : 0.726 g/mL, 0.14 mmol) of triethylamine were added to approximately 10 mL of distilled water. Into this basic solution, milligram quantities (~25 mg, FW: 168.21 g/mol, 0.15 mmol) of 2-(methylthio)benzoic acid (OS) were added to form approximately 0.14 mmol proportions of the triethylammonium 2-(methylthio)benzoate salt. Once a pH of 7 was achieved the aqueous ligand solution was reduced to a solid salt via rotary evaporation and then removed from the walls of the flask with a spatula. The salt was then redissolved in a 90/10 ethanol:H<sub>2</sub>O solution and the round bottom was equipped with a stir bar. Into the salt solution, 40 mg (FW: 628.5 g/mol, 0.06 mmol) of Rubpy(bpy(CO<sub>2</sub>CH<sub>2</sub>CH<sub>3</sub>)<sub>2</sub>)Cl<sub>2</sub>] were added along with 36 mg (FW: 252.83 g/mol, 0.14 mmol) of AgPF<sub>6</sub>. The reaction mixture was stirred and refluxed under nitrogen for 5 hours. After 1 hour, the solution turned dark red-orange and grey AgCl was seen precipitating out of solution.

After cooling to room temperature, 1-2 drops of saturated NaCl solution were added to the flask to precipitate any remaining  $\text{AgPF}_6$  and placed in the freezer overnight. The  $\text{AgCl}$  was filtered on a 15 mL fine frit and washed with ethanol. The filtrate was reduced to dryness via rotary evaporation and then precipitation was induced by addition of acetone. The precipitate was then filtered on a 30 mL medium frit to afford a dark red-orange powder. UV-vis (EtOH)  $\lambda_{\text{max}} = 463 \text{ nm}$ .

### Synthesis of $[\text{Ru}(\text{p-cymene})\text{dmbCl}]\text{Cl}$

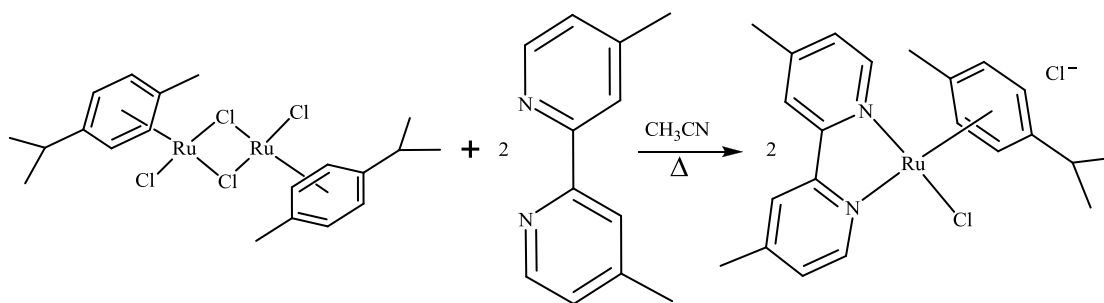


Figure 9: Synthetic scheme for  $[\text{Ru}(\text{p-cymene})\text{dmbCl}]\text{Cl}$

In a 14/20 neck 10 mL round bottom flask, equipped with a stir bar, approximately 2 mL of acetonitrile were purged with nitrogen. To the solution, 200 mg (FW: 612.39 g/mol, 0.33 mmol) of the  $[\text{Ru}(\text{p-cymene})\text{Cl}_2]_2$  dimer were dissolved along with 132.3 mg (FW: 156.18 g/mol, 1.37 mmol) of 4,4'-dimethyl-2,2'-bipyridyl. The reaction mixture was refluxed under nitrogen for 2 hours. The reaction mixture was removed from heat and cooled to room temperature while stirring for 1 hr. After 30 minutes, a bright yellow product precipitated out of solution. After cooling completely to room temperature, the dark brown supernatant solution was pipetted

from the round bottom. The mustard-yellow precipitate was filtered on a 15 mL medium frit. Yield: 326.3 mg (84.3%). UV-vis (CH<sub>3</sub>CN)  $\lambda_{\text{max}}$  = 342 nm.

<sup>1</sup>H NMR (CD<sub>3</sub>CN, 300MHz)  $\delta$ : 9.199 (d, 2H), 8.204 (s, 2H), 7.520 (d, 2H), 5.928 (d, 2H), 5.720 (d, 2H), 2.570 (m, 1H), 2.568 (s, 6H), 2.203 (s, 3 H), 1.016 (d, 6H) ppm.

### Synthesis of [Rudmb(bpy(CO<sub>2</sub>CH<sub>2</sub>CH<sub>3</sub>)<sub>2</sub>)Cl<sub>2</sub>]

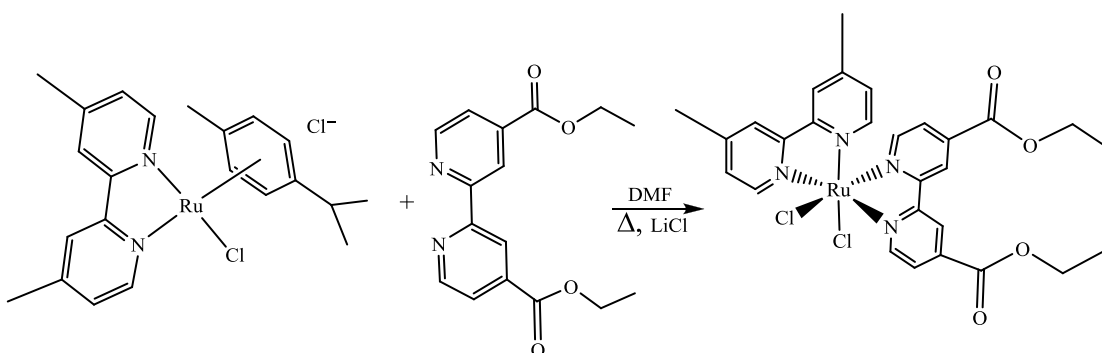


Figure 10: Synthetic scheme for [Rudmb(bpy(CO<sub>2</sub>CH<sub>2</sub>CH<sub>3</sub>)<sub>2</sub>)Cl<sub>2</sub>]

In a 14/20 neck 25 mL conical flask, equipped with a long, slender stir bar, 2.5 mL of *N,N*-dimethylformamide were purged with nitrogen gas. To the purged solution, 200 mg (FW: 490.44 g/mol, 0.41 mmol) [Ru(p-cymene)(dmb)Cl]Cl were added along with 147 mg of 2,2'-bipyridine-4,4'-diethylester. Finally, in excess of 8 equivalents of LiCl (200 mg) were added to drive the reaction. Reaction mixture was refluxed under nitrogen gas for 3 hours, during which the bright yellow reagent mixture changed to black. Reaction mixture was cooled to room temperature and crashed with acetone. Rather than pipetting acetone into conical flask, the room temperature DMF reaction mixture was poured into a 250 mL Erlenmeyer flask filled

with approximately 100 mL of cold acetone. Mixture was then filtered on a 30 mL fine frit, washed with acetone, and dried on the frit overnight to afford a brownish-black powder. Product was recrystallized with hot 1-butanol to afford a crystalline black powder.

### Synthesis of $[\text{Ru}(\text{dmb})(\text{bpy}(\text{CO}_2\text{CH}_2\text{CH}_3)_2)\text{Cl}_2]$

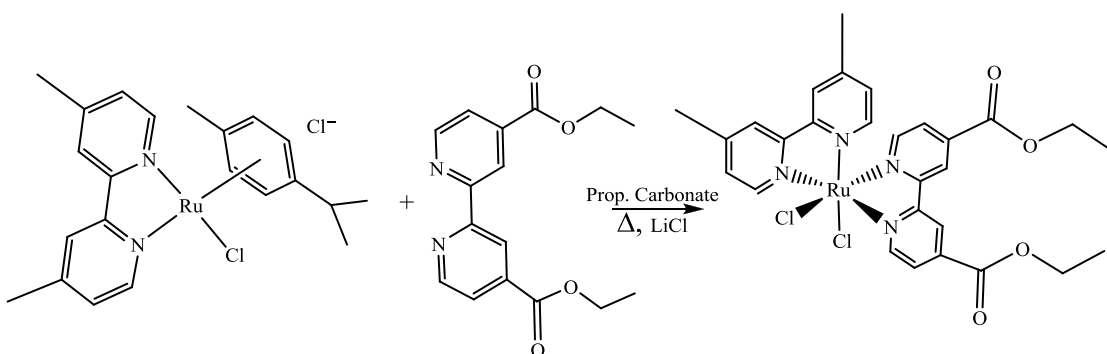


Figure 11: Synthetic scheme for  $[\text{Ru}(\text{dmb})(\text{bpy}(\text{CO}_2\text{CH}_2\text{CH}_3)_2)\text{Cl}_2]$  (propylene carbonate)

In a 14/20 neck 25 mL conical flask, equipped with a long, slender stir bar, 2 mL of propylene carbonate were purged with nitrogen gas. To the purged solution, 200 mg (FW: 490.44 g/mol, 0.41 mmol)  $[\text{Ru}(\text{p-cymene})(\text{dmb})\text{Cl}]\text{Cl}$  were added along with 147 mg of 2,2'-bipyridine-4,4'-diethylester. Finally, in excess of 8 equivalents of LiCl (200 mg) were added to drive the reaction. Reaction mixture was refluxed under nitrogen gas for 3 hours, during which the bright yellow reagent mixture changed to black. Reaction mixture was cooled to room temperature and crashed with acetone. Rather than pipetting acetone into conical flask, the room temperature reaction mixture was poured into a 250 mL Erlenmeyer flask filled with approximately 100 mL

of cold acetone. Mixture was then filtered on a 30 mL fine frit and washed with acetone.

### Synthesis of [Ru(p-cymene)biqCl]Cl

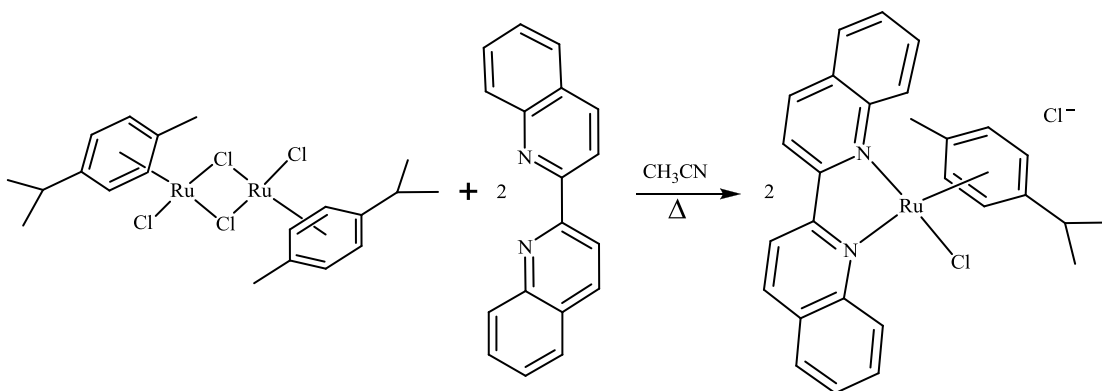


Figure 12: Synthetic scheme for [Ru(p-cymene)biqCl]Cl

In a 24/40 neck 100 mL round bottom, equipped with a stir bar, 50 mL of acetonitrile were purged with nitrogen. Then 500 mg (FW: 612.39 g/mol, 0.816 mmol) of [Ru(p-cymene)Cl<sub>2</sub>] were dissolved along with 416 mg (FW: 256.30 g/mol, 1.62 mmol) of 2,2'-biquinoline (biq). The reaction mixture was refluxed under nitrogen for 3-4 hours. Then reaction mixture volume was reduced to approximately half the volume via rotary evaporation and placed in freezer overnight to afford a pale yellow-orange plate-like, crystalline product. UV-vis (CD<sub>3</sub>CN)  $\lambda_{\text{max}} = 445$  nm. <sup>1</sup>H NMR (CD<sub>3</sub>CN, 300MHz)  $\delta$ : 8.995 (d, 1 H), 8.858 (d, 1H), 8.788 (d, 1H), 8.589 (d, 1H), 8.483 (d, 1H), 8.205 (d, 2H), 8.127 (t, 1H), 8.021 (d, 1H), 7.949 (t, 1H), 7.847 (t, 1H),

7.676 (t, 1H), 5.757 (d, 2H), 5.613 (d, 2H), 2.954 (m, 1H), 2.336 (s, 3H), 0.820 (d, 6H) ppm.

### Synthesis of [Rubiq(bpy(CO<sub>2</sub>CH<sub>2</sub>CH<sub>3</sub>)<sub>2</sub>)Cl<sub>2</sub>]

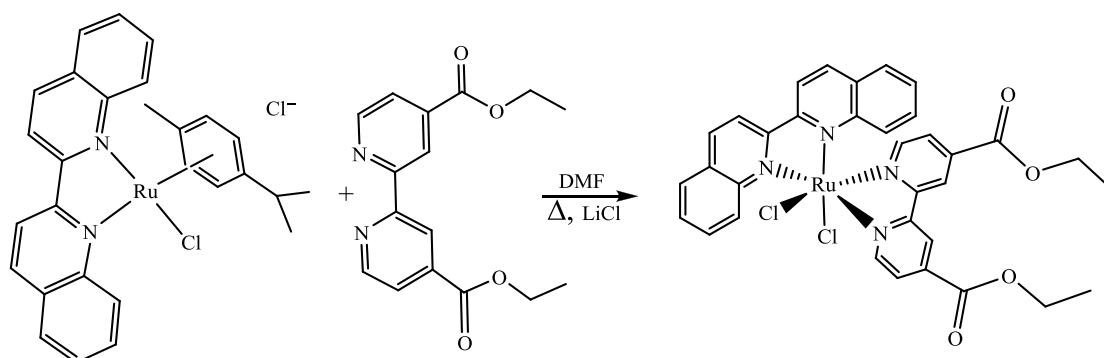


Figure 13: Synthetic scheme for [Rubiq(bpy(CO<sub>2</sub>CH<sub>2</sub>CH<sub>3</sub>)<sub>2</sub>)Cl<sub>2</sub>]

In a 14/20 neck 25 mL round bottom flask equipped with a stir bar, 2 mL DMF were purged with nitrogen. Then, 154 mg (FW: 562.49 g/mol, 0.27 mmol) of [Ru(p-cymene)biqCl]Cl were dissolved along with 98 mg (FW: 300.3 g/mol, 0.3 mmol) of 4,4'-diethylester-2,2'-bipyridine. The reaction mixture was stirred and refluxed under nitrogen for 1 ½ hours during which it changed from a pale yellow color to a dark green-black. The solution was then cooled to room temperature and precipitation was induced via addition of distilled water. The solid was filtered on a 30 mL fine frit and dried further on the Schlenk line over night. Yield: 144 mg (72.4%). UV-vis (acetone)  $\lambda_{\text{max}} = 575$  nm. <sup>1</sup>H NMR (acetone-d<sub>6</sub>, 300MHz)  $\delta$  9.200 (d, 1H), 9.032 (s, 1.5 H), 8.992 (d, 1.5 H), 8.959 (s, 1.5 H), 8.930 (s, 1H), 8.547 (d, 1.5 H), 8.312 (d, 1H), 8.261 (d, 1H), 8.175 (t, 1 H), 8.099 (d, 1H), 8.036 (s, 0.5 H), 7.996 (s, 1H), 7.991 (d, 0.5 H),

7.902 (t, 1 H), 7.728 (t, 1H), 7.142 (q, 1 H), 6.086 (d, 1H), 5.970 (d, 1H), 4.538 (m, 3 H), 1.516 (t, 4.5 H) ppm.

### Synthesis of [Rubiq(bpy(CO<sub>2</sub>CH<sub>2</sub>CH<sub>3</sub>)<sub>2</sub>)OS]

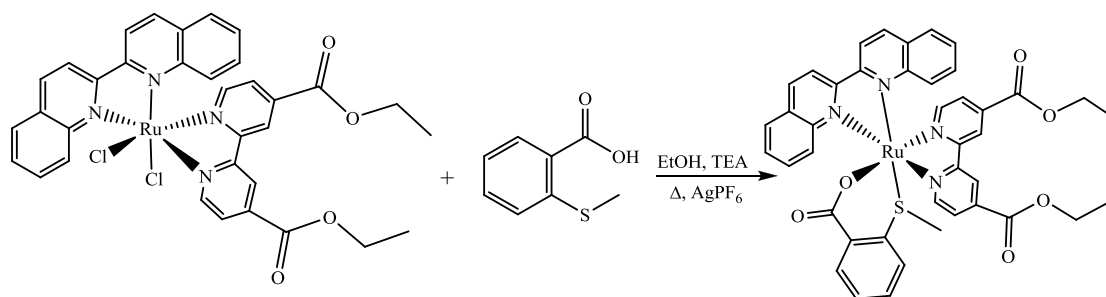


Figure 14: Synthetic Scheme of [Rubiq(bpy(CO<sub>2</sub>CH<sub>2</sub>CH<sub>3</sub>)<sub>2</sub>)OS](PF<sub>6</sub>)<sub>2</sub> (PF<sub>6</sub> counter ions omitted in scheme)

In a 14/20 10 mL round bottom flask, 6 mg (FW: 168.21 g/mol, 0.036 mmol) of 2-(methylthio)benzoic acid (OS) were dissolved in 5 mL distilled water along with dropwise amounts of triethylamine (FW: 101.19 g/mol,  $\rho$ : 0.726 g/mL) to form the triethylammonium 2-(methylthio)benzoate salt. The aqueous solution was dried to a salt via rotary evaporation and then redissolved in ethanol: The round bottom was equipped with a stir bar. Into the salt solution, 16 mg (FW: 628.5 g/mol, 0.06 mmol) of [Rubiqbpy(CO<sub>2</sub>CH<sub>2</sub>CH<sub>3</sub>)<sub>2</sub>Cl<sub>2</sub>] were added along with 36 mg (FW: 252.83 g/mol, 0.14 mmol) of AgPF<sub>6</sub>. The reaction mixture was stirred and refluxed under nitrogen overnight.

After cooling to room temperature, 1-2 drops of saturated NaCl solution were added to the flask to precipitate any remaining AgPF<sub>6</sub> and placed in the freezer for 1

hour. The AgCl solid was filtered on a 15 mL fine frit and washed with ethanol. The filtrate was reduced to dryness via rotary evaporation. The solid was then redissolved in approximately 2 mL of acetone and then precipitation was induced by addition of cold anhydrous ethyl ether.

## Ruthenium Adducts for CdSe Quantum Dot Assemblies

### Synthesis of 4,4'-di(3-chloropropyl)-2,2'-bipyridine

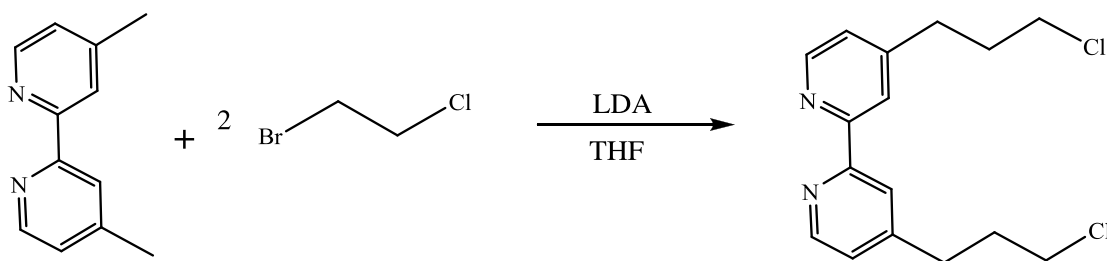


Figure 15: Synthetic scheme for 4,4'-di(3-chloropropyl)-2,2'-bipyridine

All glassware was dried in an oven overnight, capped with rubber septa, and cooled under nitrogen gas stream. All needles and cannulas were dried in an oven overnight and cooled in a desiccator. All needles, cannulas, and glassware were also flushed with nitrogen gas prior to addition of reagents due to reactivity with water and air. The verification of the n-butyllithium concentration was completed via a titration with diphenylacetic acid in dry tetrahydrofuran (THF) under nitrogen.

To a 250 mL 3-necked round bottom flask equipped with a stir bar, 40 mL dry THF was added via syringe and placed under nitrogen gas stream. Next, 4.0 mL

diisopropylamine (FW: 101.19 g/mol,  $\rho$ : 0.722 g/ml, 28.5 mmol) was added via syringe and mixture was stirred and cooled in a dry ice/acetone bath. Once cooled, 16.0 mL (FW: 64.06 g/mol, 22.4 mmol) of 1.4 M n-butyllithium in toluene were added drop by drop allowing temperature to be maintained at  $-78^{\circ}\text{C} \pm 5^{\circ}\text{C}$ . A bubbler was used to replace the volume lost due to syringe uptake of n-butyllithium.

After all n-butyllithium was added, the mixture was stirred for 10 minutes at room temperature. While stirring the lithium diisopropylamide (LDA) created in situ at room temperature, a 100 mL round bottom flask equipped with a stir bar was cooled under nitrogen stream and 1.83 g (FW: 184.29 g/mol, 9.93 mmol) of 4,4'-dimethyl-2,2'-bipyridine (dmb) were added and dissolved in 75 mL of dry THF. The LDA solution was then returned to the dry ice/acetone bath.

The dmb solution was then added via cannula to the cold LDA solution. The colorless solution immediately changed to an intensely dark brown-red color. The solution was then stirred at  $-78^{\circ}\text{C}$  for 1 hr. After stirring, 2.5 mL (FW: 143.41 g/mol, 1.723 g/mL, 30 mmol) of 1-bromo-2-chloroethane was added via syringe and stirred at room temperature overnight. Within first hour, the reaction mixture became pale orange. Within second hour, the solution precipitated a white solid.

The reaction solution polarity was changed with the addition of 30 mL saturated brine (NaCl) solution. The organic layer was washed with two 20 mL portions of dichloromethane (DCM), combined, and then washed with one 20 mL portion of brine. Finally, the solution was dried over anhydrous magnesium sulfate ( $\text{MgSO}_4$ ), filtered, and dried via rotary evaporation to afford a dark orange oil. Once

resting at room temperature for approximately an hour, the orange oil solidified. Yield: 1.52 g (50%). UV-vis (DCM): broad tail from 300 – 325 nm.  $^1\text{H}$  NMR ( $\text{CD}_2\text{Cl}_2$ , 300MHz)  $\delta$ : 8.561 (d, 2H), 8.308 (s, 2H), 7.192 (d, 2H), 3.610 (t, 4H), 3.114 (t, 4H), 2.198 (m (quintet), 4H) ppm.

### Synthesis of 2,2'-bipyridine-4,4'-dithioacetate

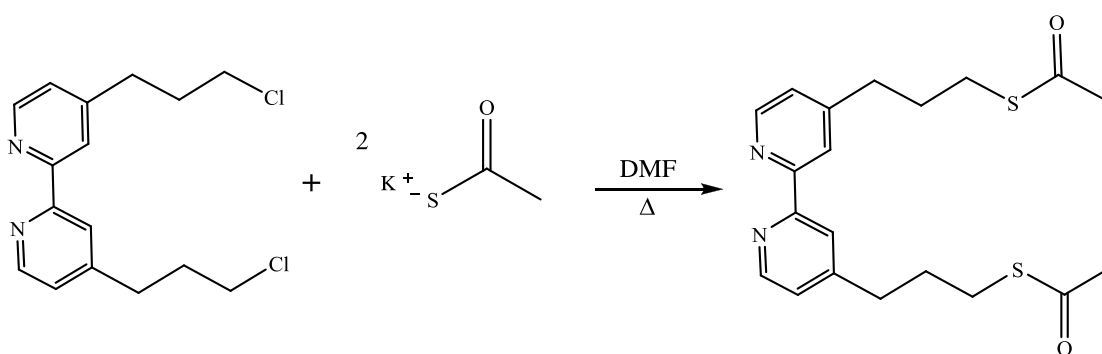


Figure 16: Synthetic scheme for 2,2'-bipyridine-4,4'-dithioacetate (bpySAC)

In a 250 mL round bottom flask equipped with a stir bar, 1.54 g (FW: 114.21 g/mol, 13.5 mmol) potassium thioacetate were dissolved in 70 mL DMF along with 1.00 g (FW: 309.00 g/mol, 3.24 mmol) 4,4'-di(3-chloropropyl)-2,2'-bipyridine. The solution was heated in an oil bath overnight at 75°C under nitrogen. The bpySAC solution was concentrated to approximately 5 mL under the vacuum line, then redissolved in dichloromethane and washed with two 10 mL portions of water. The solution was then dried over  $\text{MgSO}_4$ , filtered, and concentrated via rotary evaporation. Any residual DMF was removed by the vacuum line to afford a dark red, brown viscous liquid. Yield: 1.22 g (97%, some mass still due to adsorbed DMF). UV-vis

(DCM)  $\lambda_{\max} = 409$  nm.  $^1\text{H NMR}$  ( $\text{CD}_2\text{Cl}_2$ , 300MHz)  $\delta$ : 8.517 (d, 2H), 8.252 (s, 1H), 7.137 (d, 2H), 2.910 (t, 4 H), 2.794 (t, 4H), 2.300 (s, 6 H), 1.965 (m (quintet), 4 H) ppm.

### Synthesis of $[\text{Ru}(\text{bpy})_2(\text{bpySAC})](\text{PF}_6)_2$

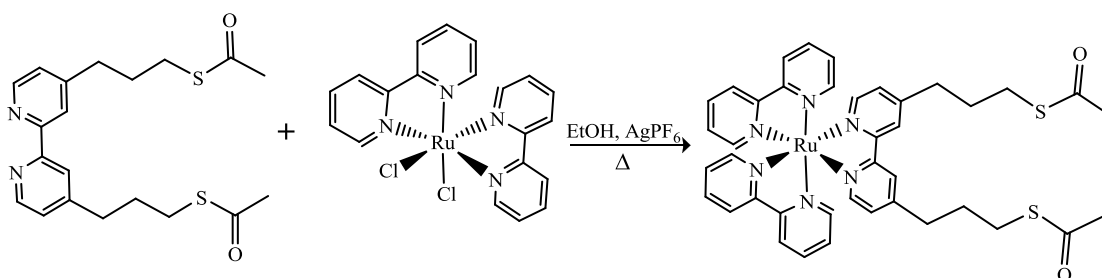


Figure 17: Synthetic scheme for  $[\text{Ru}(\text{bpy})_2(\text{bpySAC})](\text{PF}_6)_2$  (counter ions of  $\text{H}_2\text{O}$  and  $\text{PF}_6$  were omitted in scheme)

In a 50 mL conical flask equipped with a stir bar, 25 mL ethanol were purged with nitrogen. Then to the purged solution, 0.220 g (FW: 388.54 g/mol, 0.56 mmol) of bpySAC were combined with 0.349 g (FW: 520.38 g/mol, 0.67 mmol) of  $[\text{Ru}(\text{bpy})_2\text{Cl}_2] \cdot 2\text{H}_2\text{O}$  and 0.340 g (FW: 252.83 g/mol, 1.34 mmol)  $\text{AgPF}_6$ . The reaction was brought to reflux under nitrogen for approximately 4 hours. The precipitated  $\text{AgCl}$  was filtered on a fine frit and washed with ethanol. Any excess  $\text{AgPF}_6$  was filtered on a fine frit and washed with ethanol. Any excess  $\text{AgPF}_6$  was precipitated with 1-2 drops of saturated brine solution. The filtrate was then rotavapped to dryness and scraped from the round bottom flask. UV-vis ( $\text{EtOH}$ )  $\lambda_{\max} = 453$  nm.  $^1\text{H NMR}$  ( $\text{CD}_3\text{CN}$ , 300MHz)  $\delta$ : 8.509 (d, 4H), 8.429 (s, 2H), 8.063 (t, 4H),

7.718 (s, 4H), 7.545 (d, 2H), 7.418 (q, 4H), 7.243 (d, 2H), 4.124 (m, 4H), 2.920 (m, 8H), 2.380 (s, 6H) ppm.

### Synthesis of $[\text{Ru}(\text{bpy})_2(4,4'\text{-dithiopropyl-2,2'}\text{-bipyridine})](\text{PF}_6)_2$

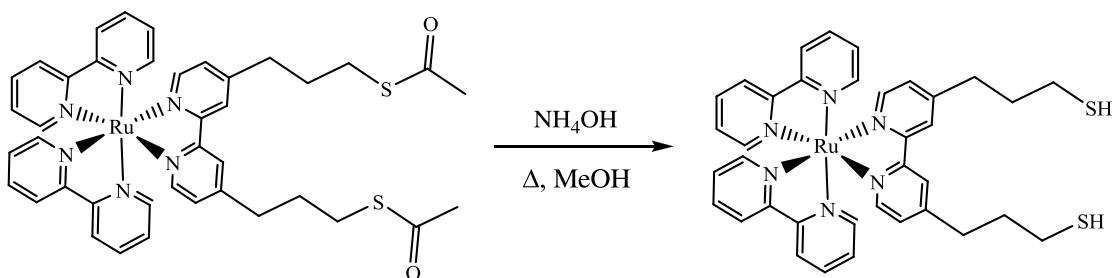


Figure 18: Synthetic scheme for  $[\text{Ru}(\text{bpy})_2(4,4'\text{-dithiopropyl-2,2'}\text{-bipyridine})](\text{PF}_6)_2$

In a 10 mL round bottom flask equipped with a stir bar, 77 mg (FW: 1090.72 g/mol, 0.071 mmol) of  $[\text{Ru}(\text{bpy})_2(\text{bpySAc})](\text{PF}_6)_2$  were dissolved in 8 mL of purged methanol. Then 20  $\mu\text{L}$  (FW: 35.05 g/mol,  $\rho$ : 0.92 g/cm<sup>3</sup>, 0.524 mmol) of concentrated  $\text{NH}_4\text{OH}$  were added via micropipette and refluxed under nitrogen for 4 hours.

To the cooled reaction mixture, 1.5 mL of 0.1 M aqueous hydrochloric acid and 5 mL of deionized  $\text{H}_2\text{O}$  were added and mixture was extracted with three 10 mL portions of dichloromethane, and then finally washed with 15 mL brine. Organic layers were collected, dried over  $\text{MgSO}_4$ , filtered, and concentrated by rotary evaporation to afford a dark brown powdery solid. UV-vis (benzonitrile and chloroform)  $\lambda_{\text{max}} = 455$  nm.  $^1\text{H}$  NMR ( $\text{CD}_3\text{CN}$ , 300MHz)  $\delta$ : 8.509 (d, 4H), 8.429 (s, 2H), 8.063 (t, 4H), 7.718 (s, 4H), 7.545 (d, 2H), 7.418 (q, 4H), 7.243 (d, 2H), 4.124 (m, 4H), 2.920 (m, 8H) ppm.

## **Photochemical Studies Sample Preparation:**

### **Steady state luminescence:**

All photoluminescence experiments were completed in 10 mm pathlength quartz fluorescence cuvettes equipped with rubber septa. All emission measurements were performed at room temperature.

### **[Ru(bpy)<sub>2</sub>(4,4'-dithiopropyl-2,2'-bipyridine)](PF<sub>6</sub>)<sub>2</sub> Coupled to 2.5 nm ( $\lambda_{\text{max}}$ = 516 nm) Cadmium Selenide Nanocrystal Quantum Dots**

All Cadmium Selenide nanocrystal quantum dots (CdSe NQDs) were obtained from Dr. Greg Van Patten's physical chemistry group. The dots were washed minimum of two times with chloroform, stored in chloroform, and sealed under argon. The concentration of the quantum dot solution as well as given diameter of the molecule was determined via the absorbance extinction coefficient at  $\lambda_{\text{max}} = 516$  nm. All molarity determinations were completed using the algorithms published in the Chem. Mater. Rev. paper which outline how to calculate the diameter, molar extinction coefficient, and concentration from the  $\lambda_{\text{max}}$  value. The published formula and effective calculations are included in the results and discussion below.

The [Ru(bpy)<sub>2</sub>(4,4'-dithiopropyl-2,2'-bipyridine)](PF<sub>6</sub>)<sub>2</sub> complex was stored as a powder, placed on the Schlenk vacuum line for five hours to remove any residual adsorbed solvent. Within an hour of photochemical studies, then it was dissolved in benzonitrile to create a concentrated stock solution. The concentration of the

ruthenium complex solution was determined via the absorbance extinction coefficient at  $\lambda_{\text{max}} = 455 \text{ nm}$ .

Emission scans of steady state luminescence were attained with excitations of 400 nm and 500 nm. The emission scan with an excitation of 400 nm was swept from 430 nm to 750 nm. The emission scan with an excitation of 500 nm was swept from 515 nm to 750 nm.

The sample blank contained 2 mL of benzonitrile and 2 mL of chloroform measured via micropipette. The ruthenium complex concentrated solution was added drop wise and diluted with a 1:1 volume solution of benzonitrile to chloroform until an absorbance of 0.28 at  $\lambda_{\text{max}} = 455 \text{ nm}$  was achieved, with approximate total volume of 4 mL. The CdSe NQD concentrated solution was added drop wise and diluted with a 1:1 volume solution of benzonitrile to chloroform until an absorbance of 0.15 at  $\lambda_{\text{max}} = 516 \text{ nm}$  was achieved, with approximate total volume of 4 mL. The Ru-CdSe NQD mixture was prepared via addition of ruthenium stock solution dropwise to an approximately 3.5 mL solution of 1:1 benzonitrile to chloroform, until 0.28 at  $\lambda_{\text{max}} = 455 \text{ nm}$  was attained. As the ruthenium complex has near zero absorbance at the quantum dot at the wavelength of 516 nm, CdSe NQD concentration could then be easily determined via dropwise addition of CdSe NQD stock solution, until an absorbance of 0.15 at  $\lambda_{\text{max}} = 516 \text{ nm}$  was attained. Once again, all samples were purged with nitrogen for at least 5 minutes and sealed with rubber septa before emission scans.

Emission scans for each sample (with exception of blank) were attained every hour for each sample until four hours total had evolved. UV-Vis absorbance spectra were collected after irradiation to detect changes in concentration or decomposition.

## **RESULTS AND DISCUSSION**

### **Part 1: Tris-Heteroleptic Ruthenium Solar Dyes**

In this research project, efforts were undertaken to effectively synthesize new ruthenium tris-heteroleptic solar dyes for use in DSSC devices. Alterations of reagents, utilization of different solvent systems, variable product isolation techniques were all utilized to optimize the syntheses. Exploring ruthenium tris-heteroleptic complex syntheses is extremely beneficial for all areas of materials research. Metal complexes can be proactively designed with selective and specific ligands to dissolve more readily in a prescribed solvent system, adhere to a substrate, and have various desired spectroscopic properties. In this study, the complex had to absorb broadly in the visible region and incorporate carboxylic acid moieties for adsorption onto the TiO<sub>2</sub> substrate. The secondary objective of investigating optimizing the dye syntheses to be robust and facile emerged from the clear difficulties with several of the synthetic steps.

First and foremost, the project began with six complexes in mind. Two of these complexes are shown below in Figure 19. They exhibit the carboxylic acid derivatized ligands for TiO<sub>2</sub> adsorption.

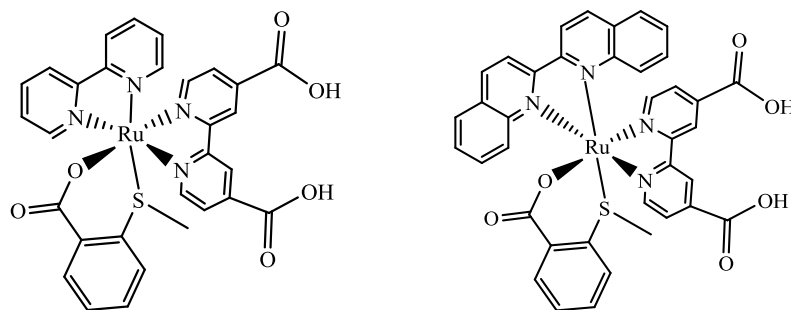


Figure 19: Two of the original target solar dye complexes

Four of the other target complexes involved the 2-(propane-2-sulfanylmethyl)pyridine (pyS) ligand (shown below along with the ligand itself) and two of these complexes were pursued by a fellow laboratory group member. The synthesis was found to be problematic due to formation of a 4-coordinate ruthenium complex impurity that dominated the recrystallization. The four-coordinate ruthenium pyS-containing complex more easily crystallized presumably due to favorable  $\pi$  stacking of the aromatic rings. Subsequently, reflecting upon these issues, the two complexes above were pursued more intently.

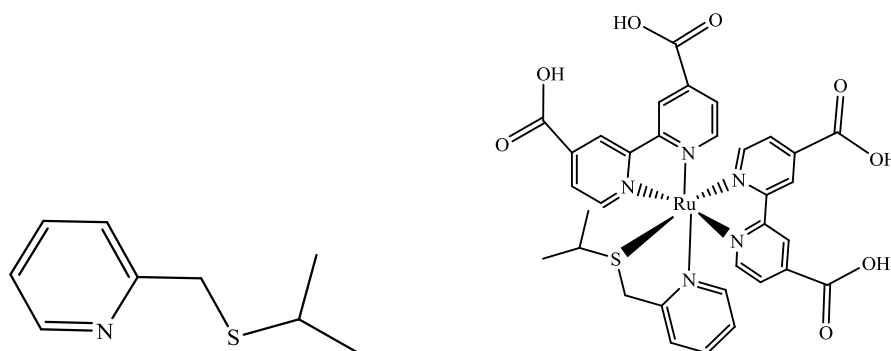


Figure 20: Molecular structure of pyS ligand and problematic solar dye complex

Throughout all of these synthetic steps, problems in separating complexes with similar solubilities arose. Inadequately separating impurities from target products would inevitably lead to reduced purity down the synthetic scheme. From previous reported syntheses for the second step of attaching the first ligand “L<sub>1</sub>” seen below, reaction concentrations were run at low concentrations in excess of acetonitrile. The reaction work-ups proved troublesome in separating the desired product, so reduced volumes of acetonitrile were utilized.

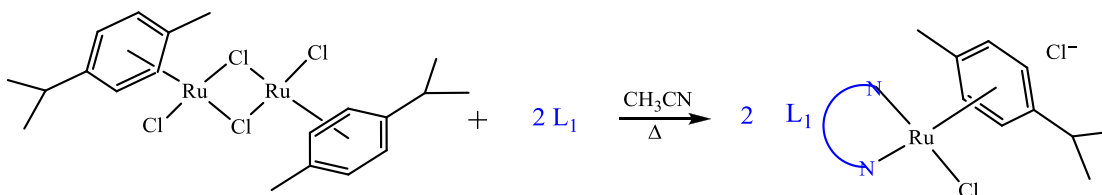


Figure 21: General synthetic scheme for [Ru(p-cymene)Cl<sub>2</sub>]<sub>2</sub> dimer to [Ru(bpy)(p-cymene)Cl]Cl synthesis

The reduced volume of acetonitrile still solvated all the reagents but the end product precipitated out of solution upon cooling to room temperature or simply once formed due to insolubility in acetonitrile. Use of reduced volume of solvent mitigated the need for an extensive product isolation procedure. Greater than 90% yields were attained for reactions ran under these conditions with high purity attained.

The most problematic reaction step in this synthetic scheme is the reaction of [Ru(p-cymene)bpyCl]Cl with L<sub>2</sub> to yield the bis chelate ruthenium dichloride compound, shown in a general scheme below: Figure 22.

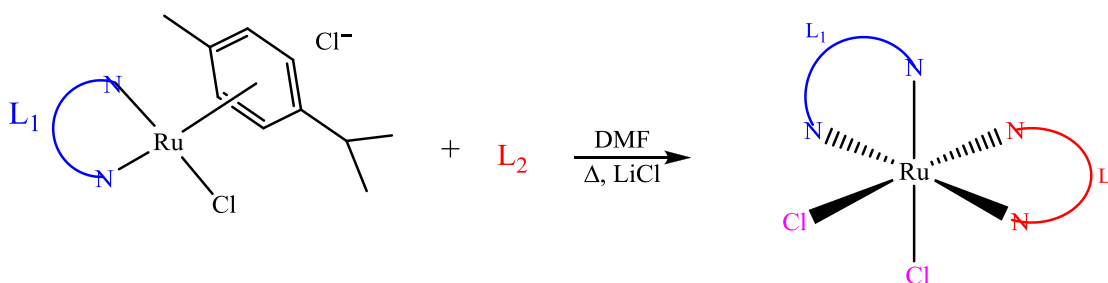


Figure 22: General synthetic scheme for  $[\text{Ru}(\text{bpy})(\text{p-cymene})\text{Cl}]\text{Cl}$  complex to  $[\text{Ru}(\text{bpy})(\text{bpy}')\text{Cl}_2]$

This reaction requires extremely high concentrations, excess equivalents of LiCl to push the reaction to product, and a high boiling point, polar aprotic solvent to allow for refluxing at high temperatures and effective solvation. *N,N'*-Dimethylformamide (DMF) solvates the reagent system most readily, but has a high coordinating ability to the transition metal center. Even high boiling point solvents with less coordination ability such as propylene carbonate, a lactone, is unable to solvate the reagents and drive the reaction to completion, resulting in very low yields. The bis DMF solvated complex however is easy to trace within the work-up as it is a deeply colored solution, either deep green for 2,2'-biquinoline derivatives or deep red for any of the 2,2'-bipyridine containing complexes. The  $[\text{Ru}(\text{L}_1)(\text{L}_2)\text{Cl}_2]$  compound, where “L<sub>1</sub>” and “L<sub>2</sub>” are the first and second ligands added respectively, is typically a black solid powder, ascribed to a broad absorbance spectrum with the highest molar absorptivity values centered around wavelength values of ~400 nm and 590 nm.

The reaction conditions and the product isolation prove quite particular for this synthesis. Whereas many reactions require indiscriminate reaction timescales, the reaction time for this synthesis has a narrow window of success. If the reaction

refluxes for less than an hour, there is still unreacted reagent. If the reaction refluxes for longer than two hours, the bis DMF substituted product is formed. UV-Visible absorbance spectrometry was utilized to monitor the growth in the absorbance bands attributed to the  $[\text{Ru}(\text{L}_1)(\text{L}_2)\text{Cl}_2]$  species; however, it must be acknowledged that the spectrum will produce small changes when pipetted hot into solvents such as methanol and ethanol due to formation of the solvent-bonded ruthenium species.

During the product isolation, the DMF bound ruthenium species can be washed away with water, but the dichloro product is also slightly water-soluble and therefore minimum aliquots of chilled water must be utilized to wash the product while filtered on the medium frit. Alternatively, the DMF bound species can also be eliminated through a recrystallization with hot 1-butanol. Butanol proves as a versatile recrystallization agent for ruthenium polypyridine complexes due to its almost amphiphilic properties of the long 4-carbon long chain and the polar alcohol group. Therefore, the solvent is able to excellently “discern” very similar species in solution.

Alterations to the synthetic scheme were pursued when it was realized that changing various ligands could provide reporters in the  $^1\text{H-NMR}$  spectrum without changing desired spectroscopic features. First, the second step of the synthetic scheme was changed to incorporate 4,4'-dimethyl-2,2'-bipyridine (dmb). The methyl groups not only provided aliphatic  $^1\text{H-NMR}$  signals, but also simplified the aromatic region by “separating” what were once four continuous vicinal protons with more complex splitting. The aromatic region of the  $^1\text{H-NMR}$  of  $[\text{Ru}(\text{dmb})(\text{p-cymene})\text{Cl}]\text{Cl}$  is shown below in Figure 23. Then, below it, the aromatic region of the  $^1\text{H-NMR}$  of

[Ru(bpy)(p-cymene)Cl]Cl shows the normal doublet, doublet, triplet, triplet splitting pattern for the 4 bipyridine protons which are symmetric with the other half of the bipyridine ligand (Figure 24). The biquinoline derivatized ruthenium has an even more extensive aromatic region, with the bulkiness of the ligand and therefore more intense through-space interactions with the other substituents creating unsymmetrical chemical shifts (Figure 25). Utilizing simpler aromatic region allowed for ease of analysis later on in the synthetic scheme, as there was no longer significant overlap of aromatic peaks in this region.

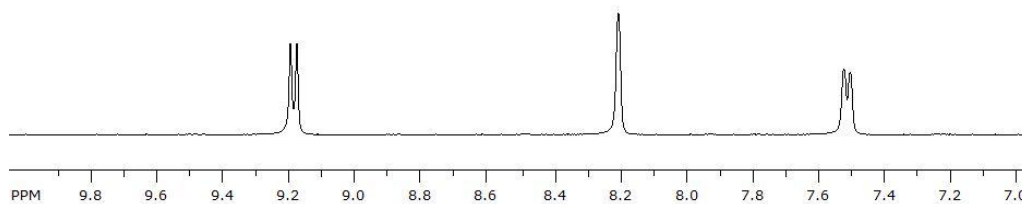


Figure 23:  $^1\text{H-NMR}$  spectrum of aromatic region: 4,4'-dimethyl-2,2'-bipyridine

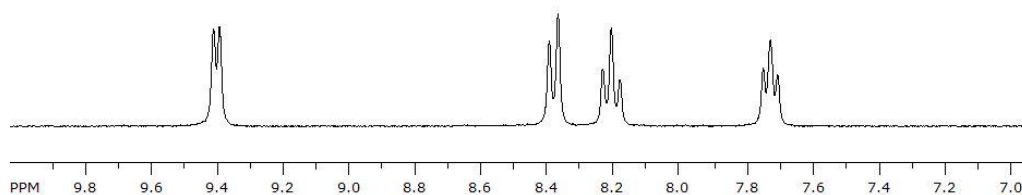


Figure 24:  $^1\text{H-NMR}$  spectrum of aromatic region: 2,2'-bipyridine

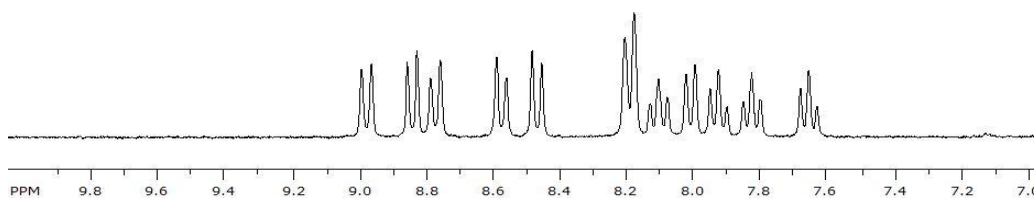


Figure 25:  $^1\text{H-NMR}$  spectrum of aromatic region: 2,2'-biquinoline

Furthermore, the carboxylic acid moieties on the bipyridine ligands produce spectra that are hard to interpret. Even after deprotonation of the carboxylic acid with dilute sodium hydroxide, the spectrum was still difficult to analyze. The synthetic scheme was therefore changed to include the use of diethyl ester derivatized bipyridines. This ligand once again provided aliphatic indicators from the ester ethyl groups. Ester ethyl groups are easy to identify due to their unique location in the spectrum downfield from most alkane features due to the ester “OCO” adjacent functional group. The ethyl ester functional group could then be easily cleaved with

base upon attaining the final tris-heteroleptic product. Finally,  $^1\text{H-NMR}$  spectra could be analyzed in a much less polar solvent such as deuterated methanol or acetone, rather than low-paramagnetic deuterated water ( $\text{D}_2\text{O}$ ) which produces difficult to interpret NMR spectra.

### **Brief Absorbance Spectral Analysis**

Once again, ruthenium polypyridine solar dyes must be highly absorbent in the visible spectrum to optimize light-harvesting capabilities. Observing the absorbance spectrum transitioning from species to subsequent species, one can see a general red-shifting of the peak absorbances (moving toward lower energy absorbance transitions showing an approaching of the potentials of the metal d orbitals and the ligand  $\pi^*$  orbitals) as well as a general broadening of the spectrum.

Shown below in Figure 26, the absorbance spectra of all the target complexes in the synthesis of  $[\text{Ru}(\text{bpy})(\text{bpy}')\text{OS}](\text{PF}_6)$  are shown. The addition of the second ligand shows the quite drastic absorbance change from the bright yellow p-cymene precursor, with a shoulder centered on  $\lambda = 405$  nm, to the broad absorbance with peak absorbances centered around 400 nm and 590 nm. Acknowledging the goal properties of the solar dyes, this complex appears to be ideal. Despite this broad absorbance, this intermediate would not serve as an adequate solar dye. First, the chloride ligands are too labile and would be prone to exchange. Secondly, the chloride ligands are  $\sigma$ -donor ligands and therefore the redox potential of the ground state ruthenium d-orbitals and the excited state predominantly ligand-character  $\pi^*$  orbitals would not be positive

enough to engage in redox reactions. Once the  $[\text{Ru}(\text{bpy})(\text{bpy}')\text{OS}]^+$  complex has been synthesized, the  $\pi$  acid (or electron pair acceptor) OS ligand pushes the ruthenium metal redox potential to more positive potentials. Thus, the dye exhibits adequate spectral coverage for light harvesting and can engage in electron transfer in a photovoltaic cell.

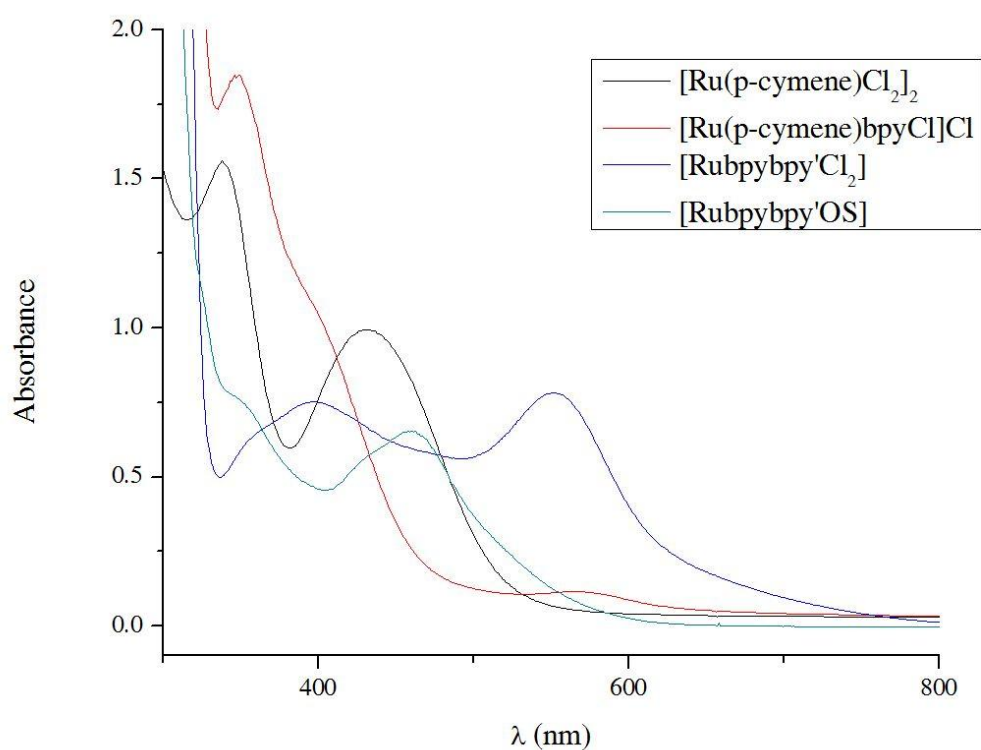


Figure 26: Absorbance spectra showing progression from  $[\text{Ru}(\text{p-cymene})\text{Cl}_2]_2$  dimer starting complex to  $[\text{Ru}(\text{bpy})(\text{bpy}')\text{OS}]$

Furthermore, UV-visible electronic transitions are governed by several selection rules: more simply, certain transitions are considered allowed, while others

are forbidden. The potential energies of the molecular orbitals formed in the metal-ligand complex binding have certain spatial properties and furthermore have certain electron occupancies. First, transitions cannot occur between orbitals of the same type of symmetry called parity. Parity involves symmetry with respect to inversion. Generally speaking, a mixing or hybridizing of orbitals relaxes this rule as one is not strictly exciting from similar parity orbitals such as  $d \rightarrow d$  transitions. And furthermore, reducing the symmetry of the ligand adducts therefore encourages this selection rule relaxing. For example, shown below in Figure 29 are the absorbance spectra for the model complex  $[\text{Ru}(\text{bpy})_3]^{2+}$ , of  $D_3$  symmetry, and for the synthesized solar dye  $[\text{Ru}(\text{bpy})(\text{bpy}')\text{OS}]^+$ , of  $C_1$  symmetry.

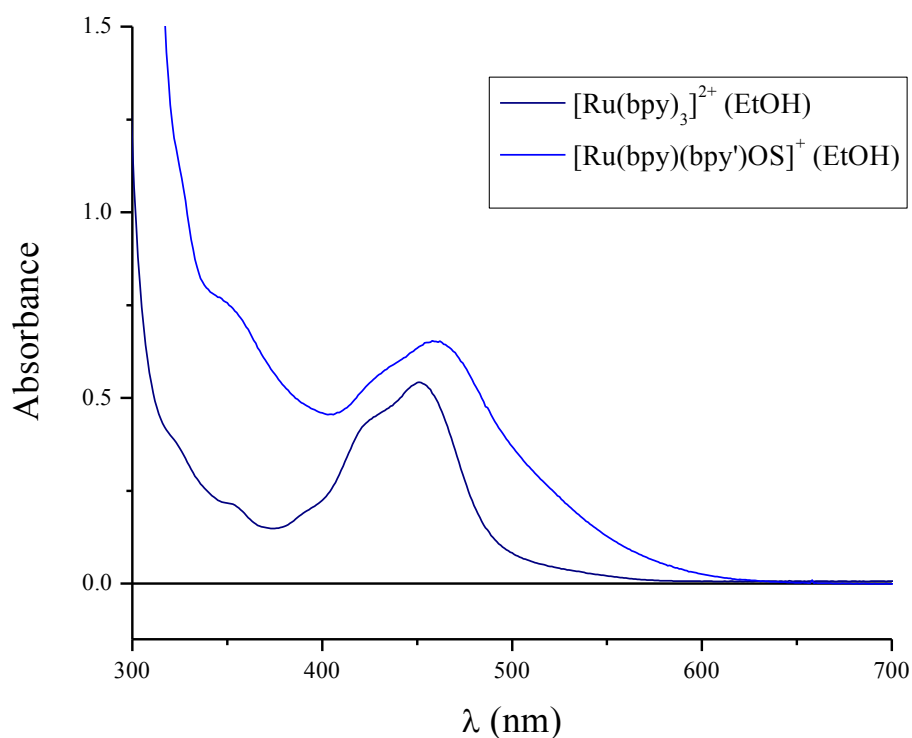


Figure 27: Comparison of absorbance spectra of  $[\text{Ru}(\text{bpy})_3]^{2+}$  and  $[\text{Ru}(\text{bpy})(\text{bpy}')\text{OS}](\text{PF}_6)$

The  $C_1$  “symmetric” solar dye (despite the symmetry in the ligands themselves) actually exhibits no metal complex symmetry. Whereas, the ruthenium tris-bipyridine complex has an axis of rotation in which three equal manipulations of  $120^\circ$  creates the identical complex. Furthermore, there is an axis of rotation perpendicular to that primary axis. The tris-heteroleptic complex’s reduced symmetry therefore enhances the electronic transitions, broadening the spectra, especially when compared to the homoleptic (containing the same ligand) species.

## **Part 2: Photochemical Analysis of Ruthenium and Quantum Dot Assemblies**

Research was undertaken to characterize the coupled electronic state of a ruthenium-cadmium selenide nanocrystal quantum dot interface utilizing absorbance and steady state luminescence spectroscopy. Several variables in the solution system can be modified. The solvents utilized, benzonitrile and chloroform, were chosen due to their miscibility across all proportions as well as ability to solvate both the hydrophobic cadmium selenide quantum dot and the charged ruthenium polypyridyl complex. However, the benzonitrile and chloroform would affect a unique solvent environment with their respective viscosities and their dielectric constants in different proportions. The size of cadmium selenide quantum dot could be altered to have

tunable absorbance and emission spectra that overlap differently with the absorbance and emission spectra of the ruthenium complex.

Furthermore, the length of the thiol terminated alkyl chains could be varied depending on the length of the dihalide alkanes utilized at the beginning of the synthesis. Finally, the concentrations and stoichiometric ratios of the Ru-CdSe NQD assembly could be varied. To reduce collisional interactions as well as to have adequate optical density for fluorescence spectrometry, low concentrations ranging from 0.01 mM to 0.0001 mM for both components were utilized. Increasing the rate of adsorption of ruthenium onto the surface of the quantum dot by increasing the ratio of ruthenium to cadmium selenide quantum dot could also be accomplished by increasing the concentration of ruthenium complex. The molar absorptivity of the ruthenium complex and cadmium selenide quantum dot are different by a factor of 7 at each respective  $\lambda_{\max}$  (for this given Ru-CdSe NQD pair). Therefore exploring the system in a 1:7 ratio of CdSe NQD:Ru could be easily achieved by attaining equitable absorbance values for each species at  $\lambda_{\max}$ . Similarly, decreasing or increasing the ratio could therefore be tailored via the proportion of the  $\lambda_{\max}$  peaks to each other.

### **Determination of Molar Absorptivity of Cadmium Selenide Nanocrystal Quantum Dots:**

Due to the inability to determine nanocrystal quantum dot solution concentration gravimetrically or by any other standard laboratory technique, molarity

is determined through a calculation from  $\lambda_{\max}$ , or the wavelength of peak absorbance that is the most red in the spectrum. More specifically, the diameter can be calculated from  $\lambda_{\max}$  and then the calculated diameter can be utilized to calculate the molar absorptivity or extinction coefficient, through a separate formula. A seminal study by Peng, et. al<sup>41</sup> that determined the algorithms for cadmium selenide, cadmium telluride, and cadmium sulfide nanocrystal quantum dots.

Function for CdSe NQD Diameter and Molar Absorptivity via  $\lambda_{\max}$  from the essential paper by Peng, Guo, Qu, et. al<sup>41</sup>

$$\text{NQD Diameter} = (1.6122 \times 10^{-9}) * \lambda_{\max}^4 - (2.6575 \times 10^{-6}) * \lambda_{\max}^3 + (1.6242 \times 10^{-3}) * \lambda_{\max}^2 - (0.4277) * \lambda_{\max} + 41.57 \text{ and}$$

$$\text{NQD Molar Absorptivity} = 5857 * d^{2.65}, \text{ where } d = \text{diameter.}$$

Therefore, for the CdSe NQDs with a  $\lambda_{\max} = 516$  nm, the diameter is equal to 2.5 nm and the molar absorptivity ( $\epsilon$ ) is equal to  $6.7E+4 \text{ cm}^{-1} * \text{M}^{-1}$ .

It is important to note that determination of ruthenium complex molar absorptivity was undertaken per normal laboratory technique in which absorbance spectra were collected at several different known concentrations of the complex; the respective absorbance at  $\lambda_{\max}$  values were recorded and then plotted against

concentration to determine the extinction coefficient. The extinction coefficient for the ruthenium complex is approximately  $1.0\text{E}+4 \text{ cm}^{-1}\cdot\text{M}^{-1}$  at XXX nm.

### **Experiment 1: Coupling with 2.5 nm CdSe NQDs in lower concentrations**

Before each photochemical study, the absorbance spectra of all species were obtained to determine concentration as well as to monitor decomposition after periods of irradiation. Figure 28 shows the absorbance spectra of the ruthenium complex, the cadmium selenide nanocrystal quantum dot, and the mixture. For nanocrystal quantum dot emission studies, an absorbance of 0.1 at  $\lambda_{\text{exc}}$  is ideal. As determined by the absorbance spectra, this study utilized a ruthenium complex solution of approximately  $2.8 \times 10^{-5} \text{ M}$ , a cadmium selenide solution of approximately  $2.2 \times 10^{-7} \text{ M}$ , and a mixture of the same concentrations for each respective species. Therefore, this study incorporated a ratio of approximately 100 ruthenium molecules for each cadmium selenide nanocrystal quantum dot.

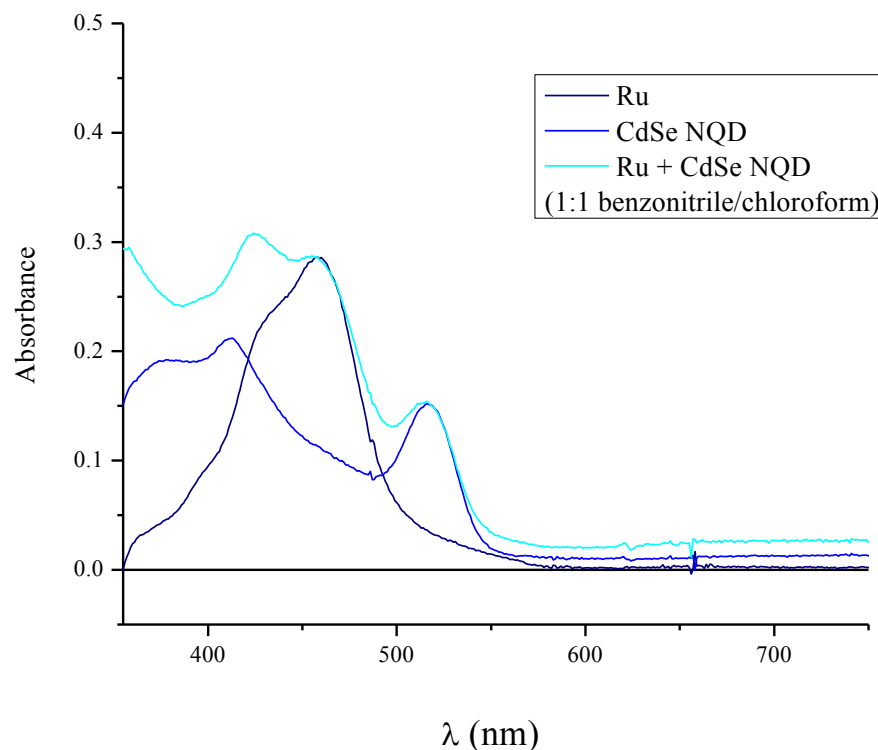


Figure 28: Absorbance spectra of  $[\text{Ru}(\text{bpy})_2(4,4'\text{-dithiopropyl-2,2'}\text{-bipyridine})](\text{PF}_6)_2$ , Cadmium Selenide Nanocrystal Quantum Dots, and the mixture

### Steady State Photoluminescence

To ensure an accurate description of the coupled system, it is essential to monitor both a blank of the solvent system alone as well as a “standard” of both the ruthenium complex and cadmium selenide quantum dot alone. The use of the standards allows for a disregard of confounding factors such as emission quenching due to solvent effects or air oxidation. In Figure 29, the emission spectra of the

ruthenium species are shown. After approximately two hours, there have been no significant changes.

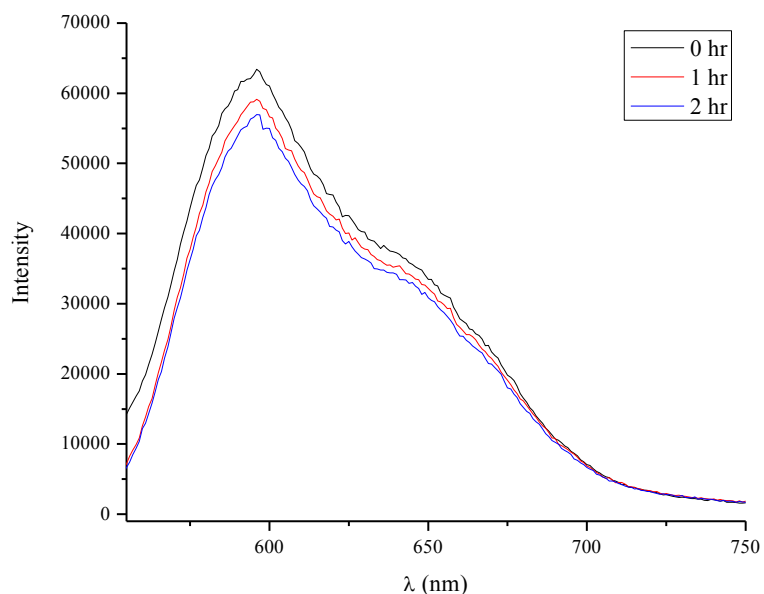


Figure 29: Steady State Photoluminescence of  $[\text{Ru}(\text{bpy})_2(4,4'\text{-dithiopropyl-2,2}'\text{-bipyridine})](\text{PF}_6)_2$ , excitation at 400 nm, in benzonitrile and chloroform

Furthermore, the sample was then irradiated with 500 nm wavelength light. The emission spectra of the ruthenium species once again after 1 hour increments is shown below in Figure 30. With 500 nm wavelength light, emission due to relaxation from the triplet metal to ligand charge transfer ( $^3\text{MLCT}$ ) state is reduced in intensity but has the same breadth. Similarly to the emission spectra shown above, there is no change in the intensity of the ruthenium based emission during the first two hours in solution.

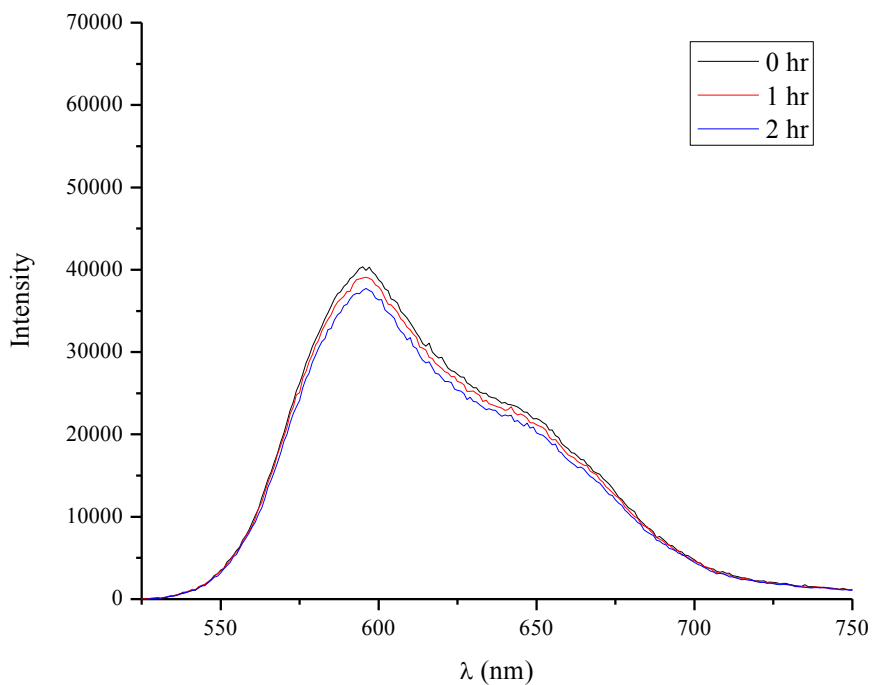


Figure 30: Steady State Photoluminescence of  $[\text{Ru}(\text{bpy})_2(4,4'\text{-dithiopropyl-2,2'\text{-bipyridine)}}](\text{PF}_6)_2$ , excitation at 500 nm, in benzonitrile and chloroform

The fluorescence of the ruthenium species and cadmium selenide quantum dots in solution should experience no decrease in emission intensity or quenching unless there is redox active species in solution. However, the coupled electronic system of the ruthenium and nanocrystal quantum dot will demonstrate changes in the emission spectra if adsorption has been accomplished. For example, shown below in Figure 31 is a schematic showing excitation of the CdSe nanocrystal quantum dot due to light absorption and effective hole transfer to the ruthenium species. Once effective hole transfer has occurred, there is a formally oxidized ruthenium species and reduced

nanocrystal quantum dot. Relaxation of the excited state electron cannot occur in the CdSe and furthermore, the Ru<sup>III</sup> species is emissively dark. Therefore, effective charge transfer would include a quenching of both the nanocrystal quantum dot emission as well as the ruthenium species. Arguably, at such excesses of ruthenium species (1:100 molar ratio in this study), there will still be emission arising from the ruthenium complex that is unbound in solution.

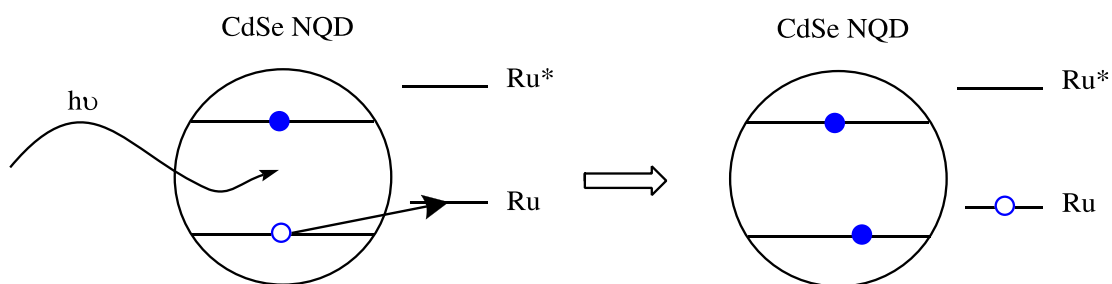


Figure 31: Schematic of electron excitation via light absorption and subsequent hole delocalization to the ruthenium complex

In Figures 32 and 33 are shown the photoluminescence spectra of the coupled system (labeled as “Mix”) and the cadmium selenide nanocrystal quantum dot. Similar to the ruthenium species in solution, the CdSe solution in benzonitrile and chloroform alone demonstrates minor quenching in the emission spectra from the hour to day long time span. More specifically, when monitored via fluorescence spectroscopy, there are minor decreases on the hour long time scale, and when irradiated via a UV lamp after days sealed in the cuvettes, emission can still be observed. Once again, the spectra at each respective wavelength of excitation show the same *pattern* of emission changes

over time, but at varying intensities. In Figures 32 and 33, the effective quenching of the cadmium selenide nanocrystal quantum dot can be observed. Notably, the emission intensity is reduced by a factor of 3 simply within minutes of mixing the solutions, purging with nitrogen, and irradiating with light in the fluorescence spectrometer.

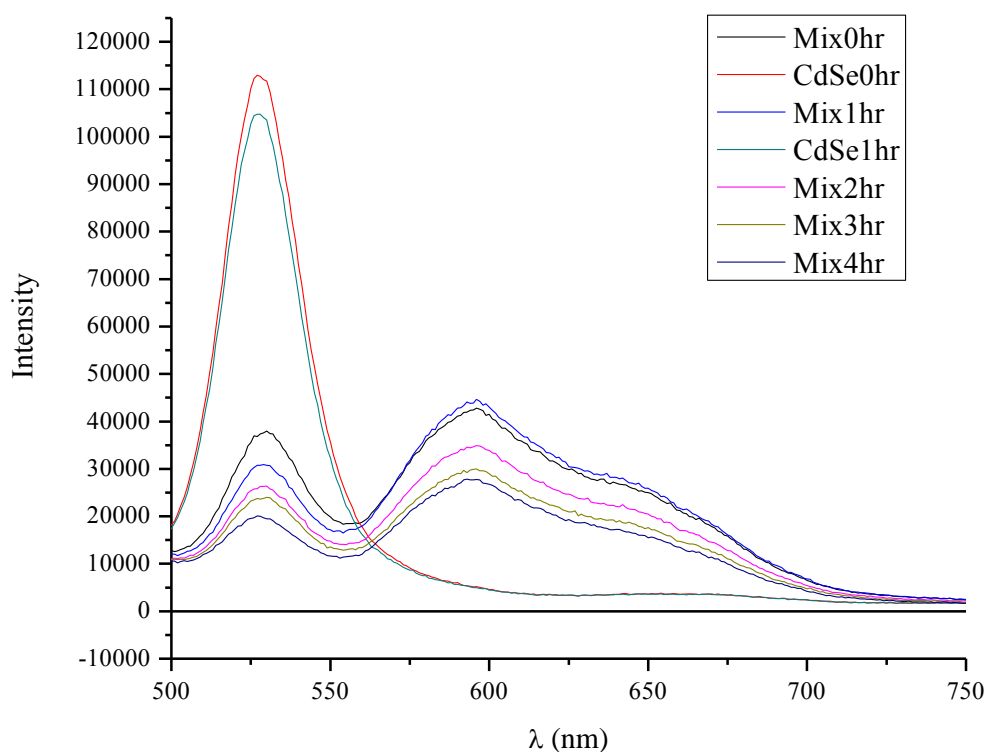


Figure 32: Steady State Photoluminescence of [Ru(bpy)<sub>2</sub>(4,4'-dithiopropyl-2,2'-bipyridine)](PF<sub>6</sub>)<sub>2</sub> and Cadmium Selenide NQD mixture as a function of time with excitation at 400 nm.

Also, for the fluorescence spectra excited at 500 nm, there is a similar diminishing of the cadmium selenide emission but with a greater magnitude of change.

Once again, after 24 hours the mixed sample only shows redder emission due to the ruthenium complex that has remained unadsorbed in solution. Arguably, there will be a point of saturation at which all empty sites on the cadmium selenide nanocrystal quantum dot that can be occupied by the ruthenium complex are.

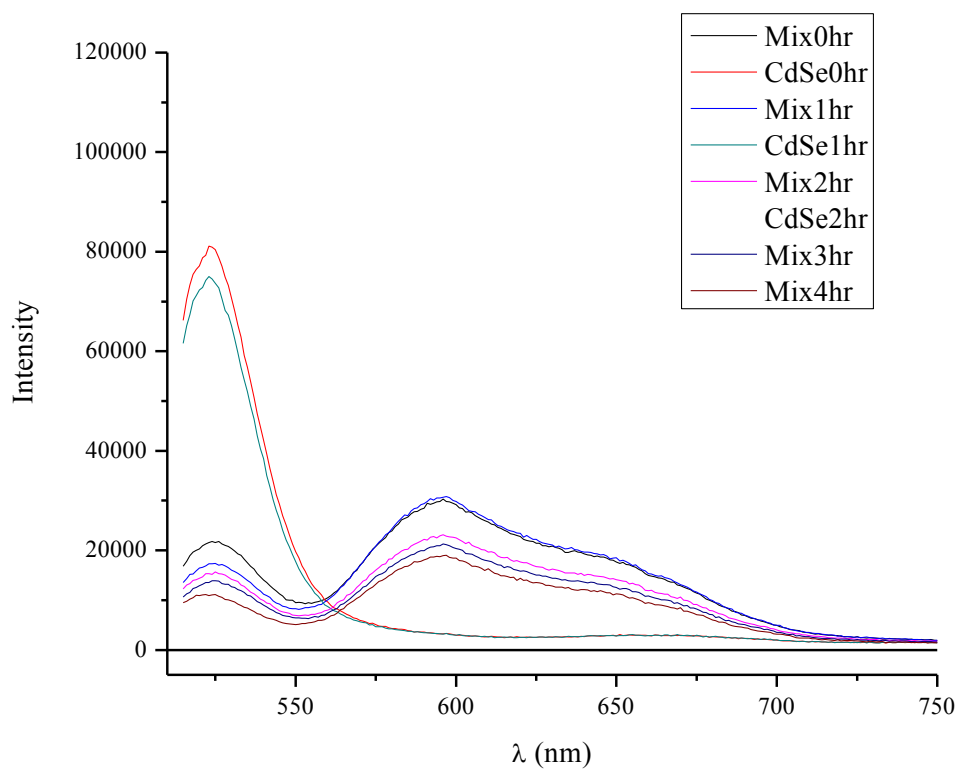


Figure 33: Steady State Photoluminescence of [Ru(bpy)<sub>2</sub>(4,4'-dithiopropyl-2,2'-bipyridine)](PF<sub>6</sub>)<sub>2</sub> and Cadmium Selenide NQD mixture, excitation at 500 nm

## CONCLUSIONS AND FUTURE DIRECTIONS

A series of ruthenium solar dyes were successfully synthesized and characterized via  $^1\text{H-NMR}$  and UV-Visible absorbance spectroscopy. The reaction conditions and product isolation procedures were explored for future tris-heteroleptic ruthenium polypyridyl work. Tris-heteroleptic syntheses are inherently more difficult to achieve due to the number of synthetic steps involved. Despite the importance of these complexes in materials research and the advantages of ligand-dependent tuning of the spectroscopic features, there is still a lacking of robust, reproducible syntheses in the literature.<sup>42,43,44</sup> One promising approach is a one-pot synthesis similar to the ruthenium p-cymene dimer method utilized in this work. In a one-pot synthesis, the same solvent (DMF) is utilized throughout the entire synthesis, ligands are added sequentially, and no product isolation occurs until the last synthetic step is complete. This method could reduce the need for cumbersome product isolation techniques.

The  $[\text{Ru}(\text{bpy})_2(\text{bpy}((\text{CH}_2)_3\text{SH})_2)](\text{PF}_6)_2$  complex was successfully synthesized. All precursors were characterized via  $^1\text{H-NMR}$  and absorbance spectroscopy. Furthermore, the final product was characterized by  $^1\text{H-NMR}$ , absorbance, and steady state luminescence spectroscopy. Molar extinction coefficients were calculated for both the cadmium selenide nanocrystal quantum dots and ruthenium complex. The system was explored through nanosecond and femtosecond transient absorption spectroscopy as well but that is outside of the scope of this written work. Furthermore,

steady state luminescence was utilized to probe emission quenching of the coupled system.

To complete the picture of this ruthenium-cadmium selenide quantum dot assembly,  $^2\text{D}$ -NMR spectroscopy studies could be completed. A synthesis of the deuterated version of the terminal alkyl-thiol ruthenium complex has been begun. This deuterated version can help elucidate the rate of adsorption of the complex to the quantum dot surface. The deuterated alkyl ligand will be “visible” through the long capping agent hydrocarbon chains. Upon adsorption of the complex onto the quantum dot surface, the deuterated protons will have different chemical shifts due to the new electronic environment of the crystalline semiconductor lattice. These studies would help illuminate the adsorption interaction between the two species.

A combination of the two research projects undertaken here could also enhance the understanding of each respective system. Tris-heteroleptic ruthenium dyes that incorporate the thiol-terminated linkers could be utilized to create supramolecular structures linking cadmium selenide quantum dots together. Besides this structural study, the thiol-derivatized ruthenium complex could be spectroscopically tuned through the addition of different ligands. We could then examine how increasing or diminishing the overlap between the absorbance spectrum of the ruthenium polypyridine dye and the emission spectrum of the nanocrystal quantum dot could alter the energy transfer mechanism.

Finally, in the spirit of the original dye sensitized solar cell architecture collaboration, more extensive interaction across chemistry sub-disciplines should be

encouraged. All areas of material research have implications in designing more energy efficient and economically viable solar energy devices.

## REFERENCES

1. Crutzen, P. J.; Geology of mankind. *Nature*, **2002**, *415*, 23.
2. Lewis, N. S.; Powering the planet. *MRS Bulletin*, **2007**, *32*, 808-820.
3. Nocera, D.G.; Lewis, N.S. Powering the planet: chemical challenges in solar energy utilization. *PNAS*, **2006**, *103*, 15729-15735. .
4. Foster, R., Ghassemi, M., Cota, A.; Solar energy: renewable energy and the environment. CRC Press, **2010**.
5. Google Public Data Explorer: World Population [http://www.google.com/publicdata/explore?ds=d5bncppjof8f9\\_&ctype=b&strail=false&nسلم=s&met\\_x=sp\\_dyn\\_le00\\_in&scale\\_x=lin&ind\\_x=false&met\\_y=sp\\_dyn\\_tfirt\\_in&scale\\_y=lin&ind\\_y=false&met\\_s=sp\\_pop\\_totl&scale\\_s=lin&ind\\_s=false&dimp\\_c=country:region&ifdim=country&iconSize=0.5&uniSize=0.035#!ctype=l&strail=false&bcs=d&nسلم=h&met\\_y=sp\\_pop\\_totl&scale\\_y=lin&ind\\_y=false&rdim=region&ifdim=region&tdim=true&tstart=30428640000&tend=1273550400000&hl=en\\_US&dl=en\\_US&ind=false](http://www.google.com/publicdata/explore?ds=d5bncppjof8f9_&ctype=b&strail=false&nسلم=s&met_x=sp_dyn_le00_in&scale_x=lin&ind_x=false&met_y=sp_dyn_tfirt_in&scale_y=lin&ind_y=false&met_s=sp_pop_totl&scale_s=lin&ind_s=false&dimp_c=country:region&ifdim=country&iconSize=0.5&uniSize=0.035#!ctype=l&strail=false&bcs=d&nسلم=h&met_y=sp_pop_totl&scale_y=lin&ind_y=false&rdim=region&ifdim=region&tdim=true&tstart=30428640000&tend=1273550400000&hl=en_US&dl=en_US&ind=false) (accessed May 10, 2012).

6. Hupp, J. T., Ryswyk, H. V., Martinson, A. B. F., Jensen, R. A., Hamann, T. W.; Advancing beyond current generation dye-sensitized solar cells. *Energy Environ. Sci.*, **2008**, *1*, 66-78.
7. U.S. Energy Information Administration: Total Energy – Primary Energy Consumption by Source. [http://www.eia.gov/totalenergy/data/annual/pecss\\_diagram.cfm](http://www.eia.gov/totalenergy/data/annual/pecss_diagram.cfm) (accessed May 6, 2012).
8. World Wildlife Fund: Change How You Live [http://www.wwf.org.uk/how\\_you\\_can\\_help/change\\_how\\_you\\_live/](http://www.wwf.org.uk/how_you_can_help/change_how_you_live/) (accessed May 15, 2012).
9. U.S. Department of Energy and National Renewable Energy Laboratory: 2010 Renewable Energy Data Book. <http://www.nrel.gov/analysis/pdfs/51680.pdf> (accessed May 10, 2012).
10. U.S. Environmental Protection Agency. Air Quality: Oil and Gas. <http://www.epa.gov/airquality/oilandgas/basic.html> (accessed May 11, 2012).
11. U.S. Environmental Protection Agency: Clean Energy. <http://www.epa.gov/cleanenergy/energy-and-you/affect/coal.html> (accessed May 12, 2012).
12. U.S. Environmental Protection Agency. Climate Change Science: Atmosphere Changes. <http://www.epa.gov/climatechange/science/recentac.html> (accessed May 11, 2012).

13. National Oceanic and Atmospheric Administration: Earth System Research Laboratory. <http://www.esrl.noaa.gov/gmd/ccgg/trends/history.html> (accessed May 11, 2012).
14. Intergovernmental Panel on Climate Change: Fifth Assessment Report. <http://www.ipcc.ch/index.htm#.T7vFUIIxPwY> (accessed May 6, 2012).
15. U.S. Environmental Protection Agency. Climate Change – Health and Environmental Effects. <http://www.epa.gov/climatechange/effects/index.html> (accessed May 11, 2012).
16. BBC World News: Science and the Environment. Study links biodiversity and language loss. <http://www.bbc.co.uk/news/science-environment-18020636> (accessed May 12, 2012).
17. Osvaldo E. S.; Chapin, F.S.; Armesto, J. J.; Berlow, E.; Bloomfield, J.; Dirzo, R.; Huber-Sanwald, E.; Huenneke, L. F.; Jackson, R. B.; Kinzig, A.; Leemans, R.; Lodge, D. M.; Mooney, H. A.; Oesterheld, M.; LeRoy, P.; Sykes, M. T.; Walker, B. H.; Walker, M.; Wall, D. H. Global Biodiversity Scenarios for the Year 2100. *Science*, **2000**, 287, 1770-1774.
18. United Nations Department of Economic and Social Affairs. <http://www.un.org/en/development/desa/index.html> (accessed May 10, 2012).
19. National Renewable Energy Laboratory. Learning About Renewable Energy: Solar Energy Basics. [http://www.nrel.gov/learning/re\\_solar.html](http://www.nrel.gov/learning/re_solar.html) (accessed May 5, 2012).

20. National Aeronautics and Space Administration. Sun: Overview. <http://solarsystem.nasa.gov/planets/profile.cfm?Object=Sun> (accessed May 6, 2012).
21. U.S. Energy Information Administration. Energy Explained: Solar Energy. [http://www.eia.gov/energyexplained/index.cfm?page=solar\\_home](http://www.eia.gov/energyexplained/index.cfm?page=solar_home) (accessed May 10, 2012).
22. University of Michigan Center for Sustainable Systems Factsheets: Photovoltaic Energy. <http://css.snre.umich.edu/publications/factsheets> (accessed May 6, 2012).
23. U.S. Energy Information Administration. Countries Proved Oil Reserves. <http://www.eia.gov/countries/index.cfm?view=reserves> (accessed May 10, 2012).
24. U.S. Energy Information Administration. Annual Energy Review: Photovoltaic Cell and Module Shipments by Type, Trade, and Price, 1982-2009 <http://www.eia.gov/totalenergy/data/annual/showtext.cfm?t=ptb1008> (accessed May 9, 2012).
25. Habas, S. E.; Platt, H. A. S.; van Hest, M. F. A. M.; and Ginley, D. Low-cost inorganic solar cells: from ink to printed device. *Chem. Rev.*, **2010**, 110, 6571-6594.
26. Nozik, A.J.; Miller, J.R., Introduction to solar photon conversion. *Chem. Rev.*, **2010**, 110, 6443-6445.

27. Gratzel, M.; Mendes, A.; Aguilar Ribeiro, H.; Nazeeruddin, M. K.; Zakeeruddin, S. M.; Andrade, L., Influence of different cations of N3 dyes on their photovoltaic performance and stability. *Intl. Jour. of Chem. Eng.*, **2009**, 1-7.
28. Gratzel, M.; O'Regan, B.; A low-cost, high-efficiency solar cell based on dye-sensitized colloidal TiO<sub>2</sub> films. *Nature*, **1991**, 353, 737-740.
29. Gratzel, M.; Humphry-Baker, R.; Nazeeruddin, Md. K.; Zakeeruddin, S. M.; Shklover, V., Stepwise assembly of tris-heteroleptic polypyridyl complexes of ruthenium(II). *Inorg. Chem.*, **1998**, 37, 5251-5259.
30. Fraser, C.L.; Demas, J.N.; Payne, S.J.; Klinkenberg, S.J.; Goguen, B.N.; Fiore, G.L. Ruthenium tris(bipyridine) complexes with sulfur substituents: model studies for PEG coupling. *Inorg. Chem.*, **2008**, 47, 6532-6540.
31. Hammarstrom, L.; Modin, J.; Davidsson, J.; Wallin, S., Femtosecond transient absorption anisotropy study on [Ru(bpy)<sub>3</sub>]<sup>2+</sup> and [Ru(bpy)(py)<sub>4</sub>]<sup>2+</sup>: ultrafast interligand randomization of the MLCT State. *J. Phys. Chem. A.*, **2005**, 109, 4697-4704.
32. Meyer, G.J.; Castellano, F.N.; Staniszewski, A.; Sun, Y.; Ardo, S., Stark effects after excited-state interfacial electron transfer at sensitized TiO<sub>2</sub> nanocrystallites. *JACS*, **2010**, 132, 6696-6709.
33. Klimov, V.I.; Meyer, T.J.; Bezel I.; Alstrum-Acevedo, J.; Petruska, M.A.; Sykora, M. Photoinduced charge transfer between CdSe nanocrystal quantum dots and Ru-polypyridine complexes. *JACS*, **2006**, 128, 9984-9985.

34. Kornberg, R.D.; Bushnell, D.A.; Ackerson, C.J.; Calero, G.; Jadzinsky, P.D. Structure of a thiol monolayer-protected gold nanoparticle at 1.1 angstrom resolution. *Science*, **2007**, *318*, 430-433.
35. Brust, M.; Bethell, D.; Hasan, M. The Fate of sulfur-bound hydrogen on formation of self-assembled thiol monolayers on gold:  $^1\text{H}$  NMR spectroscopic evidence from solutions of gold clusters. *JACS*, **2002**, *124*, 1132-1133.
36. Weiss, E. A.; Cass, L. C.; Frederick, M. T.; Morris-Cohen, A. J. Simultaneous determination of the adsorption constant and the photoinduced electron transfer rate for a CdS quantum dot-viologen complex. *JACS*, **2011**, *133*, 10146-10154.
37. Gladfelter, W. L.; Mann, K. R.; Blank, D. A.; Bohnsack, J. N.; Huss, A. S.; Rossini, J. E. Binding and static quenching behavior of a terthiophene carboxylate on monodispersed zinc oxide nanocrystals. *J. Phys. Chem. C*, **2011**, *115*, 11-17.
38. Alivisatos, A.P. Semiconductor Clusters, Nanocrystals, and Quantum Dots. *Science*, **1996**, *271*, 933-937.
39. Green, M. The nature of quantum dot capping ligands. *Jour. of Mater. Chem.*, **2010**, *20*, 5797-5809.
40. Nozik, A.J. Quantum dot solar cells. *Physica E*. **2002**, 115-12
41. Peng, X.; Guo, W.; Qu, L.; Yu, W., Experimental determination of the extinction coefficient of CdTe, CdSe, and CdS nanocrystals. *Chem. Mater.*, **2003**, *15*, 2854-2860.

42. Anderson, P. A.; Deacon, G. B.; Haarmann, K. H.; Keene, R.; Meyer, T. J.; Reitsma, D. A.; Skelton, B. W.; Strouse, G. F.; Thomas, N. C.. *Inorg. Chem.*, **1995**, *34*, 6145-6157.
43. Gratzel, M.; Zakeeruddin, S. M., Nazeeruddin, Md. K.; Humphry-Baker, R. *Inorg. Chem.*, **1996**, *37*, 5251-5259.
44. Mann, K. R.; Pomije, M. K.; Evju, J. K.; Freedman, D. A. *Inorg. Chem.*, **2001**, *40*, 5711-5715